NeuroImage 223 (2020) 117352

Contents lists available at ScienceDirect

NeuroImage

journal homepage: www.elsevier.com/locate/neuroimage

Subthalamic deep brain stimulation identifies frontal networks supporting initiation, inhibition and strategy use in Parkinson's disease

Philip E. Mosley[a,b,c,d,*], Katherine Robinson[a], Terry Coyne[c,e], Peter Silburn[b,c], Megan S. Barker[f,g], Michael Breakspear[a,h], Gail A. Robinson[c,f], Alistair Perry[a,i,j]

[a] Systems Neuroscience Group, QIMR Berghofer Medical Research Institute, Herston, Queensland, Australia
[b] Neurosciences Queensland, St Andrew's War Memorial Hospital, Level 1, St Andrew's Place, 33 North Street, Spring Hill, Queensland 4000, Australia
[c] Queensland Brain Institute, University of Queensland, St Lucia, Queensland, Australia
[d] Faculty of Medicine, University of Queensland, Herston, Queensland, Australia
[e] Brizbrain and Spine, the Wesley Hospital, Auchenflower, Queensland, Australia
[f] School of Psychology, University of Queensland, St Lucia, Queensland, Australia
[g] Taub Institute for Research on Alzheimer's Disease and the Aging Brain, Columbia University Medical Centre, New York, USA
[h] Brain and Mind Priority Research Centre, Hunter Medical Research Institute, University of Newcastle, NSW, Australia
[i] Max Planck UCL Centre for Computational Psychiatry and Ageing Research, Berlin, Germany
[j] Centre for Lifespan Psychology, Max Planck Institute for Human Development, Berlin, Germany

ARTICLE INFO

Keywords:
Deep brain stimulation
subthalamic nucleus
impulsivity
inhibition
Parkinson's disease
executive functioning

ABSTRACT

Initiation and inhibition are executive functions whose disruption in Parkinson's disease impacts substantially on everyday activities. Management of Parkinson's disease with subthalamic deep brain stimulation (DBS) modifies initiation and inhibition, with prior work suggesting that these effects may be mediated via the connectivity of the subthalamic nucleus (STN) with the frontal cortex. Here, we employed high-resolution structural neuroimaging to investigate the variability in initiation, inhibition and strategy use in a cohort of twenty-five (ten females, mean age 62.5, mean Hoehn and Yahr stage 2.5) participants undertaking subthalamic DBS for Parkinson's disease. Neuropsychological assessment of initiation and inhibition was performed preoperatively and at six months postoperatively. We first reconstructed the preoperative connectivity of the STN with a frontal network of anterior and superior medial cortical regions. We then modelled the postoperative site of subthalamic stimulation and reconstructed the connectivity of the stimulation field within this same network. We found that, at both pre- and postoperative intervals, inter-individual variability in inhibition and initiation were strongly associated with structural network connectivity. Measures of subcortical atrophy and local stimulation effects did not play a significant role. Preoperatively, we replicated prior work, including a role for the right inferior frontal gyrus in inhibition and strategy use, as well as the left inferior frontal gyrus in tasks requiring selection under conditions of maintained inhibition. Postoperatively, greater connectivity of the stimulation field with right anterior cortical regions was associated with greater rule violations and suppression errors, supporting prior work implicating right-hemispheric STN stimulation in disinhibition. Our findings suggest that, in Parkinson's disease, connectivity of the frontal cortex with the STN is an important mediator of individual variability in initiation and inhibition,. Personalised information on brain network architecture could guide individualised brain circuit manipulation to minimise neuropsychological disruption after STN-DBS.

1. Introduction

1.1. Deep brain stimulation as a tool to understand brain function

Deep brain stimulation (DBS) is a method of brain manipulation that enables targeted, focal modulation of brain activity in close proximity to the stimulating electrode. As well as these local stimulation effects, DBS can also modulate activity in distant brain regions that are anatomically connected to the surgical target. Beneficial and adverse effects of DBS can be related to stimulation at both the focal and distal, network level. Importantly, DBS can be a tool that illuminates the mechanistic role of these brain regions and networks in health and disease. Careful measurement of longitudinal changes in behavioural or symptom profiles arising after DBS can be related to the site and distribution of

* Corresponding author at: Neurosciences Queensland, St Andrew's War Memorial Hospital, Level 1, St Andrew's Place, 33 North Street, Spring Hill, Queensland 4000, Australia.
E-mail address: philip.mosley@qimrberghofer.edu.au (P.E. Mosley).

https://doi.org/10.1016/j.neuroimage.2020.117352
Received 30 April 2020; Received in revised form 22 July 2020; Accepted 4 September 2020
Available online 9 September 2020
1053-8119/

stimulation in order to characterise brain circuit dysfunction. Parkinson's disease is a neurodegenerative disorder in which DBS is established as an advanced treatment for motor symptoms and in which network effects associated with clinical effectiveness have previously been delineated (Accolla et al., 2016; Vanegas-Arroyave et al., 2016; Akram et al., 2017; Horn et al., 2017; Chen et al., 2018). Notably, Parkinson's disease is also a model neuropsychiatric disorder (Weintraub and Burn, 2011), although the anatomical determinants of non-motor symptoms have received much less attention. In this study, we investigate a group of regulatory or '*executive*' cognitive functions that are affected by neurodegeneration in Parkinson's disease and may also be disrupted by DBS of the subthalamic nucleus (STN), the most common surgical target for DBS in this disorder. We employ high-resolution diffusion magnetic resonance imaging (dMRI) to model the distribution of white matter tracts in the brain and examine connections of the surgical target site that mediate network-wide effects of DBS. We also examine whether changes in executive functioning are also related to local stimulation effects within the STN and subcortical grey matter neurodegeneration.

1.2. Initiation, inhibition and strategy use in Parkinson's disease

Initiation and inhibition are executive functions supported by the frontal cortex (Fuster, 2015). An adaptive agent balances these processes, such that stimulus-response associations rapidly generate behaviour when appropriate, but automatic responses are supressed when alternative actions with greater value are available. In Parkinson's disease, problems with the initiation of action give rise to cardinal motor symptoms such as rigidity and bradykinesia. In the non-motor domain, initiation deficits are associated with apathy, a cognitive and emotional syndrome characterised by diminished goal-directed behaviour and diminished interest (Starkstein et al., 1992; Starkstein and Brockman, 2011). However, persons with Parkinson's disease may also have problems with inhibition (Gauggel et al., 2004; Kobayakawa et al., 2008; Obeso et al., 2011; Nombela et al., 2014), manifest as the inability to withhold an action, independent of the known effects of dopaminergic replacement medication on compulsive choice (Antonelli et al., 2014). Spatially-extensive white matter pathology in fronto-striatal circuits is present in the early clinical stages of Parkinson's disease and may underlie these distributed cognitive deficits (Rae et al., 2012).

Previous work testing clinical participants with lesions of the prefrontal cortex has identified specific anatomical substrates of these processes (Aron et al., 2004b). Initiation can be measured using the construct of energization, the attentional process that underpins the initiation and maintenance of a verbal response (Barker et al., 2018). Timed word fluency tasks are commonly used to assess energization, during which responses must be initiated and maintained after a starting cue. If the process of energization is defective, responding slows over time, akin to '*running out of steam*' (Robinson et al., 2015b). Energization impairments are associated with damage to the anterior and superior medial frontal lobes including the anterior cingulate cortex and pre-supplementary motor cortices (Alexander et al., 2005; Stuss et al., 2005; Picton et al., 2007; Shallice et al., 2007, 2008). In Parkinson's disease, dopaminergic depletion may also impair energization resulting in a quantitative reduction in effortful activity (McAuley, 2003). Deficits in verbal fluency have been reported from the early stages of Parkinson's disease (Lees and Smith, 1983).

Energization is also implicated in the production of spontaneous, narrative speech, during which the addition of each new piece of semantic or conceptual information demands re-recruitment of attentional processes. Energization deficits lead to delayed initiation and longer pauses in persons with Parkinson's disease, which have also been associated with grey matter atrophy in ventromedial prefrontal regions (Ash et al., 2012).

Initiation interacts synergistically with inhibition to facilitate efficient performance in language tasks. Effective inhibition allows for the rapid selection of one response when multiple competing verbal responses are linked to the same cue. Competition-induced conflict impairs sentence generation in individuals with lesions of the left inferior frontal gyrus (Robinson et al., 2010) and this effect is most marked for phonemic over semantic verbal fluency (Robinson et al., 2012). This is consistent with the role of the inferior frontal gyrus in an inhibitory prefrontal network comprising the supplementary motor area and the subthalamic nucleus (Aron et al., 2007).

The Hayling sentence completion test (Burgess et al., 1997) assesses verbal initiation and inhibition in the same task. In section one (the initiation condition), the examiner delivers fifteen sentences with the last word missing. Participants must complete the sentence with a word that is meaningful, as quickly as possible (e.g. *the captain stayed with the sinking… ship*). In section two (the suppression condition), the examiner delivers fifteen further sentences. Participants must now insert a word that is not semantically related to any natural completion (e.g. *the whole town came to hear the Mayor… banana*), whilst also responding as quickly as possible. Participants are penalised for completing the sentence with clearly related words such as '*speak*', or '*talk*' (referred to as category A errors), as well as with words that are only partially connected such as '*explode*' (referred to as category B errors). Successful performance on the Hayling test thus requires the inhibition of prepotent responses in section two, after initiating their rapid production in section one. An additional skill that may be recruited for successful performance is the ability to generate and implement a strategy, in order to rapidly select unconnected words in section two (e.g. items from a category such as fruit: '*banana*', '*orange*', '*apple*' or items visible in the examination room: '*desk*', '*chair*', '*pen*').

In persons with frontal brain lesions, the pattern of deficits observed in the Hayling test suggests distinct cortical regions associated with these different aspects of Hayling performance. Slowed performance during the straightforward initiation condition is associated with right ventromedial prefrontal lesions, slowed performance in the suppression condition with lesions of the right inferior frontal gyrus, and suppression errors with lesions of the right orbitofrontal cortex (Volle et al., 2012). In a subsequent study, lesions of the right inferior frontal gyrus were also associated with a higher number of (semantically-related) category B errors and fewer correct responses that derived from a strategy (Robinson et al., 2015a). In hierarchical terms, it is hypothesised that this failure to implement a strategy leads to longer thinking times in the suppression condition and difficulty inhibiting incorrect prepotent responses. Again, the role of the inferior frontal gyrus suggests recruitment of the aforementioned inhibitory '*stopping*' network in this task (Aron, 2011). These findings have been supported amongst persons with Parkinson's disease, who make more category A and B errors than controls on this task (Obeso et al., 2011) and in whom suppression errors are associated with grey matter atrophy in medial orbitofrontal cortex, right lateral orbitofrontal cortex and right inferior frontal gyrus (O'Callaghan et al., 2013a).

The excluded letter fluency (ELF) task is a further method of assessing both verbal initiation and suppression. Participants are given three trials of ninety seconds to produce as many words as possible that do not contain a specified vowel. Words must be longer than three letters, must not be proper nouns and must not be derivations of the same stem (e.g. '*drive*', '*driver*', '*driving*'). The ELF yields an overall correct score and a rule violation score (i.e. words containing the excluded letter and those breaking the additional aforementioned constraints). In Parkinson's disease, rule violations are associated with grey matter atrophy in medial orbitofrontal cortex and left inferior frontal gyrus (O'Callaghan et al., 2013b).

1.3. The subthalamic nucleus, Parkinson's disease and deep brain stimulation

The subthalamic nucleus (STN) is a subcortical, glutamatergic, excitatory, relay nucleus that increases the inhibitory drive of the basal ganglia and suppresses action. It is of central relevance to initiation and

inhibition in healthy populations (Rae et al., 2015), as well as the pathophysiology of Parkinson's disease. In Parkinson's disease, STN neurons display abnormal patterns of burst firing as a consequence of dopaminergic denervation (Vila et al., 2000) and low-frequency synchronisation of local field potentials with cortical regions (Brown et al., 2001; Eusebio et al., 2009). Interruption of these synchronous oscillations with subthalamic deep brain stimulation (STN-DBS) is an established treatment for the motor symptoms of Parkinson's disease (Eusebio et al., 2011; Shimamoto et al., 2013). Through interrupting a pathological elevation in inhibitory outflow from the basal ganglia, STN-DBS reduces tremor, rigidity and bradykinesia, improves quality of life and permits reduction or cessation of dopaminergic therapies (Krack et al., 2003; Williams et al., 2010; Schuepbach et al., 2013).

The effects of STN-DBS on non-motor aspects of initiation and inhibition are, however, variable and may be modulated by differential effects of stimulation on the fronto-striatal networks supporting these cognitive processes. The STN is a small nucleus and receives many overlapping direct cortical projections from the frontal lobe, forming a '*hyperdirect*' pathway through which the cerebral cortex can access the basal ganglia output nuclei directly, bypassing the striatum (Nambu et al., 2000). These cortico-STN afferents display a ventromedial to dorsolateral topography, parcellating the STN into an affective component in the ventromedial tip, a cognitive-associative STN in the medial aspect and a motor component in the posterior and lateral region (Lambert et al., 2012; Haynes and Haber, 2013; Accolla et al., 2014; Ewert et al., 2018). Dispersion of the stimulation field from a DBS electrode, even one accurately placed in the motor subregion, can modulate non-motor circuits mediating cognition rather than movement. Therefore, disrupting the inhibitory role of the STN in these domains with DBS may have unwanted cognitive and affective effects.

Consequently, STN-DBS has been linked to impulsivity, the pathophysiology of which may lie in the function of the STN as a '*stopping*' node in the cognitive as well as the motor domain (Jahanshahi et al., 2015; Mosley and Marsh, 2015). In computational terms, physiological STN firing delays decision-making, allowing time for evidence accumulation and the formulation of an appropriate behavioural strategy (Doll and Frank, 2009). Accordingly, overriding this function with DBS unmasks impulsive and error-prone responding (Frank et al., 2007; Cavanagh et al., 2011). Following STN-DBS, persons with Parkinson's disease execute erroneous actions (Hershey et al., 2004) and take longer to cancel an action (Obeso et al., 2013), suggesting an impairment in action restraint. Recent work suggests that these non-motor side effects depend upon the local distribution of the stimulation field within the STN, with stimulation of the cognitive-associative STN subregion associated with postoperative disinhibition (Mosley et al., 2018b). However, spread of stimulation into associative and limbic subregions may not be the only mediators of adverse neuropsychiatric side effects, which may also include modulation of white matter tracts traversing adjacent to the nucleus, such as the medial forebrain bundle (Coenen et al., 2009, 2012).

As regards initiation, performance in both semantic and phonemic verbal fluency may worsen after subthalamic DBS (Parsons et al., 2006; Witt et al., 2008; Combs et al., 2015). This postoperative impairment may relate to surgery-independent factors such as ageing and the progression of neurodegeneration (Daniels et al., 2010), postoperative reduction of dopaminergic therapies unmasking apathy (Thobois et al., 2010), or to penetration of the caudate nucleus during lead implantation and stimulation outside of the optimal motor subregion of the STN (Witt et al., 2013).

1.4. Initiation, inhibition and the structural connectivity of prefrontal networks

The anatomical correlates of cognitive dysfunction in Parkinson's disease can be assessed using the regional distribution of atrophy in cortical and subcortical areas. However, techniques such as voxel-based morphometry yield discrepant findings (Camicioli et al., 2009; Lee et al., 2010; Nishio et al., 2010; Song et al., 2011) and may suffer methodological limitations including a reduced sensitivity to spatially complex and subtle findings (Davatzikos, 2004). Diffusion MRI (dMRI) is a neuroimaging technique that may be best suited to characterising the anatomical underpinnings of cognitive changes driven by neurodegeneration, as well as the distributed effects of targeted stimulation within subcortical structures. It models the architecture of white matter tracts in the brain (Jbabdi et al., 2015), and has previously been employed to model dimensional variations in impulsivity in Parkinson's disease (Mosley et al., 2019).

In this study, we investigate the variability in initiation and inhibition in a cohort of participants undertaking STN-DBS for Parkinson's disease. Using high-resolution preoperative diffusion MRI data, we reconstruct the connectivity of a prefrontal network centred upon the STN as a hub. Using a multivariate statistical path-modelling technique, we characterise the contribution of particular cortical regions within this network to different behavioural aspects of initiation and inhibition. After STN-DBS, we reconstruct the distribution of subthalamic stimulation and model the network-wide effects of DBS, using a simulated volume of activated subthalamic tissue as the hub of this network. We then identify white matter tracts associated with postoperative variability in these executive functions. These non-motor associations complement the existing literature delineating motor networks associated with clinically-effective STN-DBS (Accolla et al., 2016; Vanegas-Arroyave et al., 2016; Akram et al., 2017; Horn et al., 2017; Chen et al., 2018). Furthermore, we model regional stimulation effects within the STN, allowing us to delineate the contributions of distant connectivity versus local stimulation effects in the aetiology of these findings. Finally, we assess whether postoperative variability in initiation and inhibition is related to network structure at baseline, and whether neural '*disease progression*' (manifest with a specific subcortical pattern of atrophy observed in individuals with Parkinson's disease) affects these outcomes (Zeighami et al., 2015; Yau et al., 2018).

2. Materials and methods

2.1. Participants

Prior to the commencement of data collection, the full protocol was approved by the Human Research Ethics Committees of the Royal Brisbane & Women's Hospital, the University of Queensland, the QIMR Berghofer Medical Research Institute and UnitingCare Health. All participants gave written, informed consent to participate in the study.

Consecutive recruitment occurred at the Asia-Pacific Centre for Neuromodulation in Brisbane, Australia in 2018 at the time of assessment for subthalamic deep brain stimulation. All participants met the UK Brain Bank criteria for Parkinson's disease (Hughes et al., 1992). All participants were at Hoehn and Yahr stage 2 or greater (Hoehn and Yahr, 1967) with motor fluctuations or other motor complications related to dopaminergic therapy. One participant had a levodopa-resistant tremor. Candidates meeting the Movement Disorder Society criteria for dementia were excluded (Emre et al., 2007). The disease subtype was established based on an analysis of the dominant symptoms elicited during the Unified Parkinson's Disease Rating Scale (UPDRS) Part III Motor Examination, as described in Spiegel et al. (2007). In this investigation, assessments took place prior to DBS ('*on*' medication) and six months postoperatively ('*on*' stimulation).

2.2. Neuropsychological assessment

2.2.1. Verbal fluency

Participants completed phonemic (letter) and semantic (category) word fluency tasks for one minute each. In the phonemic fluency task, participants generated as many words as possible (excepting proper nouns and numbers) beginning with F, A and S and the total number of

correct responses for each letter was summed. In the semantic fluency task, participants were asked to name as many animals as possible.

2.2.2. Spontaneous speech

Two tasks designed to elicit connected speech were administered – a picture-elicited narrative and a self-generated narrative. The pictorial scene was the Beach Scene from the Queen Square Screening Test for Cognitive Deficits (Warrington, 2010). Participants were given one minute to '*describe what is happening in this picture'* and the total number of words generated was summed. In the self-generated narrative task, participants were given one minute to describe their favourite holiday. Speech samples were digitally recorded and transcribed to include all words, sounds and repeats. Non-words (e.g. '*um*'), habitual starters (e.g. '*let's see'*), questions to the examiner (e.g. '*is that enough*?') and comments on the task (e.g. '*this is hard'*) were not counted in the total number of words.

2.2.3. Energization

The total number of words generated on the verbal fluency and spontaneous speech tasks were separated into the number generated in the first fifteen and the last forty-five seconds. An energization ratio was calculated as the number of words produced in the last forty-five seconds as a proportion of the total in sixty seconds.

2.2.4. Hayling test

Performance on the Hayling test yielded scaled scores based on the response time to produce a meaningful word in section one (initiation response time) or a word that was not semantically connected in section two (suppression response time), as well as an overall scaled score based on a combination of response times and suppression errors. Scaled scores ranged from one to ten, corresponding with normative percentiles: 1 = < 1st percentile; 10 => 99th percentile. Suppression errors in section two were distinguished by category A (clearly connected) and B (somewhat connected) responses. Category B responses included those connected by their semantic relationship to the *expected response* (e.g. *the dough was put in the hot... freezer*), to the *sentence* (e.g. *the dough was put in the hot… bread*) or by their bizarre or socially inappropriate relationship to the sentence (e.g. *the whole town came to hear the major… cry*). Hayling A and B errors were summed (with category A errors weighted more heavily) to return a global error score (each A error is worth 3 points and each B error is worth 1 point). Three measures were employed to assess for the use of a strategy. Firstly, correct (nonsense) responses in section two (termed category C responses) were categorised according to whether or not the participant used an obvious strategy, including the use of items visible within the testing room (e.g. *the dough was put in the hot… desk*) and items semantically connected to previous responses (e.g. *the dough was put in the hot… apple*; previous response: *orange*). Secondly, a ratio for category A suppression errors related errors on the last ten items of section two against errors on all fifteen items, under the assumption that participants with a strategy would make fewer A errors after the first five trials. Finally, the difference between the raw response times (suppression – initiation) was calculated to provide an additional metric of strategic efficiency, under the hypothesis that the lack of a consistent strategy would lead to longer response times in section two of the task.

2.2.5. Excluded letter fluency

Participants were given three trials of ninety seconds each to produce as many words as possible that did not contain a specified letter: '*A*', '*E*' and '*I*'. Additional rules were that words must be longer than three letters, must not be proper nouns and must not be derivations of the same word stem. Participants were given examples of inappropriate words and were asked to generate words without the letter '*S*' as a practice. Participants were reminded of the rules in between each trial. An overall total correct score was recorded, as well as the number of rule violations.

2.3. Image acquisition

A preoperative T1-weighted MPRAGE, a T2-weighted FLAIR sequence and diffusion-weighted imaging (DWI) were obtained using a 3T Siemens Prisma and a 64-channel head coil. Briefly, the acquisition parameters were as follows: *T1*, 1 mm^3 voxel-resolution, TR = 2000 ms, TE = 2.38 ms, flip angle = 9°, matrix size = 256 × 256, FOV = 256 × 256 × 192; *T2*, 1 × 1 × 2 mm voxel-resolution, TR = 9500 ms, TE = 122.0 ms, flip angle = 120°, matrix size = 256 × 256, FOV = 256 × 256 × 70; *DWI,* 90 directions, *b*-value = 3000s/mm^2, voxel size = 1.7 mm^3 isotropic. Twelve non-diffusion-weighted images (*b*0) were interleaved throughout this main diffusion sequence, while an additional sequence of 8 *b*0 images were also collected with the opposite phase-encoding (posterior-anterior) direction. Postoperative CT images for all participants were acquired on a Siemens Intevo, with a resolution of 0.5 mm^3.

The DWI data were pre-processed with MRtrix3 (https://github.com/MRtrix3/mrtrix3), using an in-house preprocessing pipeline (https://github.com/breakspear/diffusion-pipeline). Preprocessing steps included denoising (Veraart et al., 2016), correction for motion, susceptibility, and eddy-current induced distortions (Andersson and Sotiropoulos, 2016) and bias-intensity correction (Zhang et al., 2001; Smith et al., 2004). Full details on DWI acquisition, preprocessing and fibre reconstruction are provided in Supplementary Information: Methods and Supplementary Fig. 1) and have been previously published (Mosley et al., 2019).

2.4. Tractography & apparent fibre density

Using the preoperative DWI data, constrained spherical deconvolution (CSD) (Tournier et al., 2004, 2007; Jeurissen et al., 2014) was performed in each participant after group-average intensity normalization (Raffelt et al., 2012), furnishing voxel-wise estimates of fibre orientation distribution functions (fODF). Using the STN as a seed, fibre tracts to target regions were reconstructed with the probabilistic streamline algorithm iFOD2 (Tournier et al., 2010). Estimates of structural connectivity between each seed and target region were derived from the *apparent fibre density* (AFD) representing the underlying intra-axonal volume (Raffelt et al., 2012). For each pathway of interest, the AFD was calculated by summing the fODF lobe integrals, approximating the total fibre volume, then dividing by the mean streamline length.

2.5. Preoperative network connectivity

The influence of prefrontal structural connectivity on initiation and inhibition prior to DBS was evaluated using a frontal network previously employed to investigate impulsivity and gambling behaviour (Mosley et al., 2019), and comprising cortical regions previously shown to be implicated in these neuropsychological functions (Fig. 1A). Cortical targets were derived from a subdivision of the cortex based on multimodal MRI data (Glasser et al., 2016). These included areas 10r and 10v (ventromedial prefrontal cortex - vmPFC), OFC and pOFC (orbitofrontal cortex - OFC), a24 and p24 (anterior cingulate cortex - ACC), 45 and 47l (inferior frontal gyrus - IFG), 6ma and 6mp (pre-supplementary motor area - SMA). The STN served as the seed within this tractography network, derived from Ewert et al. (2018). Using Advanced Normalization Tools (ANTs) (Avants et al., 2008), all parcellations were non-linearly transformed into native diffusion space via the skull-stripped anatomical image.

2.6. Surgery & stimulation titration

After the STN was manually identified on FLAIR imaging, bilateral implantation of Medtronic 3389, Boston Vercise or Abbott 6172 directional electrodes took place in a single-stage procedure using a Leksell stereotactic apparatus. Intraoperative microelectrode recordings (MER)

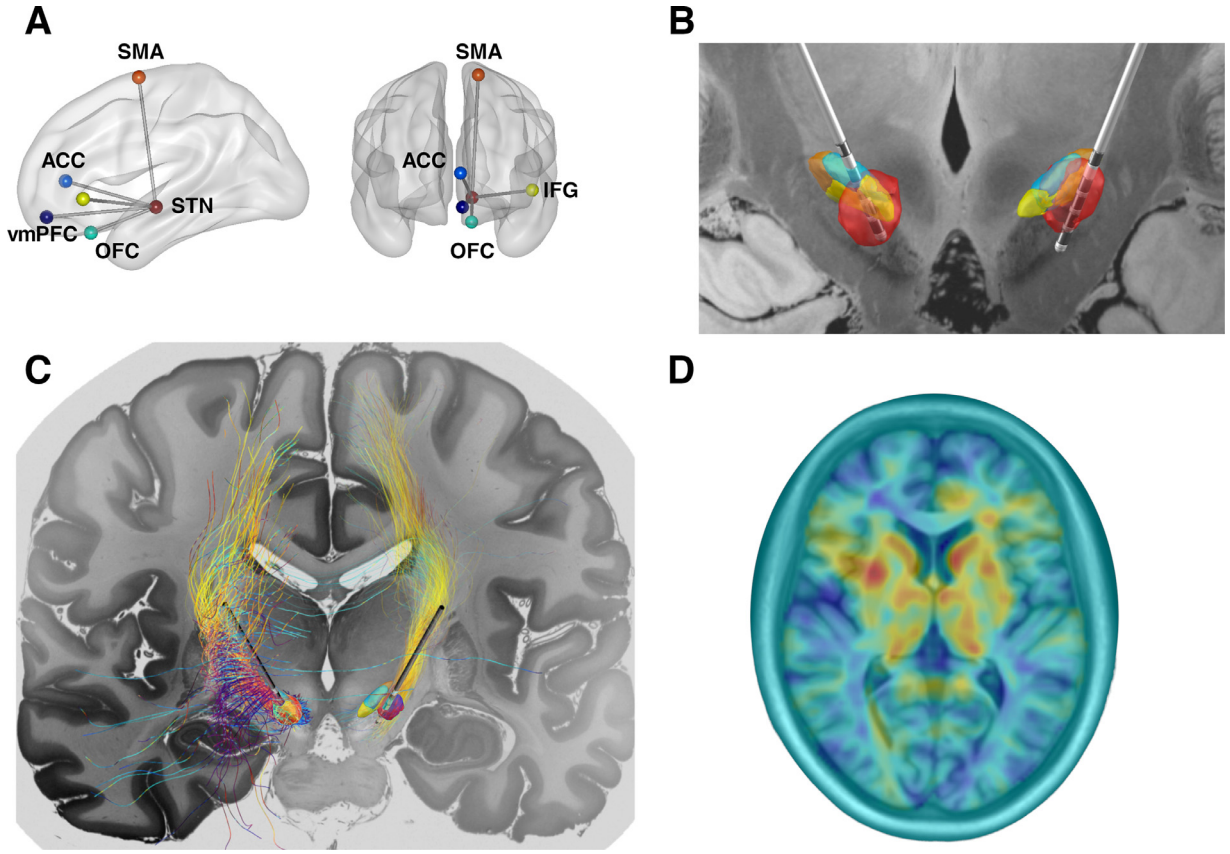

Fig. 1. Brain network reconstruction.
A: Nodes and edges of the frontal network connecting the STN with ACC, IFG, OFC, SMA and vmPFC. Network models were visualised with the BrainNet Viewer (Xia et al., 2013). B: Subthalamic electrodes were identified on postoperative imaging and electrodes were localised in ICBM 2009b nonlinear asymmetric space using the Lead-DBS toolbox. Stimulation volumes (red) were estimated for each participant based on individual stimulation parameters. The local distribution of the stimulation field within affective (yellow), cognitive-associative (blue) and motor (brown) subregions of the STN (Ewert et al., 2018) was estimated. C: Postoperatively, the subthalamic VAT replaced the STN as the hub of the frontal network and the structural connectivity of the VAT within the network was calculated as in Mosley et al. (2020). In this figure, streamlines are overlaid on a single-subject 7-Tesla MRI at 100 micron resolution (Edlow et al., 2019). D: Atrophy scores were calculated for each participant using disease based morphometry, with reference to an intrinsic brain network comprising subcortical and brainstem regions that is atrophic in early Parkinson's disease (Zeighami et al., 2015).
ACC = anterior cingulate cortex, IFG = inferior frontal gyrus, OFC = orbitofrontal cortex, SMA = pre-supplementary motor area, STN = subthalamic nucleus, vmPFC = ventromedial prefrontal cortex, VAT = volume of activated tissue.

were employed to identify the boundaries of the STN and intraoperative test stimulation was performed. Postoperative lead placement was confirmed with CT imaging. Subthalamic stimulation was commenced immediately with the initial choice of contact based upon MER signals. After discharge, participants returned to the clinic at set intervals for further titration of stimulation (including changes in stimulating contact) until motor symptoms were satisfactorily treated without adverse effects. Dopaminergic medication was reduced or ceased postoperatively, with dose of remaining treatment converted to a levodopa-equivalent daily dose (LEDD) value (Evans et al., 2004). All participants had obtained stable stimulation settings at six months postoperatively and no participants manifested any clinically-significant psychiatric symptoms as a result of stimulation.

2.7. Electrode localisation & volume of tissue activation

DBS electrodes were localized using the Lead-DBS toolbox (Horn and Kuhn, 2015; Horn et al., 2019) (https://github.com/netstim/leaddbs/tree/develop). Preoperative structural acquisitions were co-registered with postoperative CT imaging and then normalized into common ICBM 2009b nonlinear asymmetric space using the SyN approach implemented in ANTs (Avants et al., 2008). Electrode trajectories were reconstructed after correcting for brainshift in postoperative acquisitions by applying a refined affine transform in a subcortical area of interest calculated pre- and postoperatively. Rotation of directional electrodes was determined based on visualization of the artefact created by the orientation marker and directional electrode segments (Hellerbach et al., 2018). For each electrode, a volume of activated tissue (VAT) was estimated using a volume conductor model of the DBS electrode and surrounding tissue, based on each participant's individualised stimulation settings and a finite element method to derive the gradient of the potential distribution (Horn et al., 2019). In Australia, MR imaging is contraindicated with DBS electrodes in situ and therefore the simulated VAT was applied to the structural connectivity data acquired preoperatively.

2.8. Postoperative network connectivity & local subthalamic stimulation

The distributed influence of the subthalamic site of stimulation on structural networks pertaining to initiation and inhibition was evaluated using the same preoperative frontal networks, but now with the STN replaced by the subthalamic VAT as the hub of each network (Fig. 1B and also described in Mosley et al. (2020)). The purpose of this step was to specifically identify those subthalamic-prefrontal connections that were

incorporated in the stimulation field (and hence were stimulated by the implanted electrodes), so that the direct influence of stimulation on postoperative behaviour could be quantified. Notably, this could include connections from within the subthalamic nucleus but also from adjacent fibre tracts encompassed by a stimulation field extending outside of the boundaries of the nucleus. Both types of connections could be important in the genesis of postoperative variability in executive function. In order to contrast the role of distal, structural connectivity (STN and peri-STN) with focal stimulation within the STN, we also modelled the distribution of the subthalamic stimulation field within STN subregions. The overlap of the stimulation field within the STN was estimated with reference to a multimodal parcellation of the STN into *limbic, associative* and *motor* subregions (Ewert et al., 2018), as in (Mosley et al., 2018b) (Fig. 1C). For both hemispheres, the extent of each subregion volume occupied by each participant's simulated VAT was calculated (for pipeline see https://github.com/AlistairPerry/DBSVATstats).

2.9. Disease-based morphometry & assessment of disease progression

Previous work has identified an intrinsic brain network comprising subcortical and brainstem regions that is atrophic in early Parkinson's disease (Zeighami et al., 2015). Neurodegeneration may spread from this '*disease reservoir*' network to affect strongly connected cortical regions, including bilateral frontal lobes (Yau et al., 2018). This network (obtained from https://neurovault.org/images/12551) was resampled into MNI 2009c nonlinear space and masked to included only grey matter populations (Fig. 1D). Each participant's skull-stripped image was nonlinearly co-registered with the MNI PD25 atlas (http://nist.mni.mcgill.ca) and the resulting deformation warps were used to calculate the voxel-wise local volumetric change (the Jacobian determinant). Mean deformation values within the atrophic network were calculated after smoothing with a 2 mm Gaussian kernel to yield an atrophy score (for pipeline see https://github.com/AlistairPerry/PDdiffusion).

2.10. Data analysis

Where univariate statistical testing was employed, results were corrected for multiple comparisons using the Benjamini and Hochberg method (1995), with $q = 0.05$.

2.10.1. Principal components analysis

Principal components analysis (PCA) was first performed on the neuropsychological test scores in order to identify principal modes of variation amongst initiation, inhibition and strategy use. This reduced the dimensionality of the data set, given the potential for redundancy in the assessment of these constructs. In addition, dimension reduction ensured the following statistical analysis was well posed, given the relatively large number of measures and the modest number of participants. Amongst Hayling items assessing strategy use, the total number of strategic category C responses was inverted to maintain a consistent valence with the category A error ratio and the suppression–initiation response time difference. Components of the PCA with eigenvalues greater or equal to one were retained for further analysis.

2.10.2. Partial least squares path modelling

Partial least squares path modelling (PLS-PM) was employed to represent the multivariate relationships between connectivity, atrophy, subthalamic stimulation and behavioural measures (McIntosh and Lobaugh, 2004; Shaw et al., 2016). PLS-PM is a form of structural equation modelling in which linear associations between multivariate data sets can be estimated. Each model specifies the linear weighting of one set of variables that best co-varies with a linear weighting of another. In this investigation, we were interested in how brain structure (connectivity) affected executive functioning (behaviour) and whether this was also influenced by age, duration of disease, dopaminergic medication, a subcortical measure of disease progression and postoperative local stimulation effects within the STN. A connectivity variable within the path model was constructed from the AFD of each white matter tract in the frontal network and the individual contribution of each tract to the connectivity variable was quantified by a '*weight*' (linear coefficient). Behavioural variables were formed from each dimension of the PCA. The relationship between the connectivity and behavioural variables was quantified in the path model by a path coefficient and tested for statistical significance using bootstrapping, in which the data set was repeatedly sampled with replacement to create 10,000 independent bootstrapped data sets. Age, years since diagnosis of Parkinson's disease, LEDD (calculated both pre- and postoperatively), and the subcortical atrophy score were entered as co-variates. As dopamine agonist medication may have more impact upon executive functioning than levodopa, the equivalent agonist-only dose was additionally included. The interaction (or moderating) effect of subcortical atrophy on connectivity was also modelled. For all postoperative models, a local subthalamic stimulation variable was created as a weighted mixture of the overlap of each stimulation field within each subthalamic subregion. A depiction of these models is provided in Supplementary Fig. 2 and further information on PLS path modelling is provided in Supplementary Information: Methods). In order to identify the contribution of each tract to individual variability in the construct under examination, individual weights from the connectivity variable are reported, as well as the R^2 value prior to bootstrapping, which was used as the summary metric of overall model fit.

2.10.3. Atrophy scores and cross-lagged modelling

Two methods were used to evaluate whether postoperative variability in initiation and inhibition, in addition to being influenced by the site and connectivity of subthalamic stimulation, was also associated with pre-existing morphological changes related to neurodegeneration and structural connectivity at baseline. Firstly, the individual atrophy scores derived from disease-based morphometry were entered into the postoperative PLS-PM model as a unique anatomical variable. Secondly, the connectivity of fronto-subthalamic tracts that were highly-weighted in the postoperative model (i.e. fibres passing through the simulated subthalamic VAT) were entered into a cross-lagged panel model, in order to evaluate whether structural connectivity of these tracts at baseline influenced behaviour postoperatively (Supplementary Fig. 3 and Supplementary Information: Methods).

These latent change score models assess longitudinal associations between two or more repeatedly sampled measures of brain and behaviour (Kievit et al., 2018; Muetzel et al., 2018; Lin et al., 2019). They quantify cross-domain coupling, capturing the extent to which change (Δ) in one domain (initiation and inhibition) reflects the baseline level in the other (connectivity) and vice versa. Here, a bivariate cross-lagged model described four brain-behaviour relations of interest. These comprised: connectivity-behaviour covariance at baseline ($Connectivity_{t1} \sim Behaviour_{t1}$), connectivity to behaviour coupling ($Connectivity_{t1} \rightarrow \Delta Behaviour$), behaviour to connectivity coupling ($Behaviour_{t1} \rightarrow \Delta Connectivity$) and an estimate of correlated change in connectivity and behaviour ($\Delta Connectivity \sim \Delta Behaviour$) after taking into account the coupling pathways. Change in connectivity ($\Delta Connectivity$) was defined as the change in network connectivity after the subthalamic VAT was added as a seed for probabilistic tractography. In the context of the present investigation, we were mainly interested in the ability of pre-DBS network connectivity to predict cognitive change from pre- to post-DBS ($Connectivity_{t1} \rightarrow \Delta Behaviour$). Model fit metrics comprised the Comparative Fit Index (CFI - the degree to which the proposed model better fits the data than one that assumes no correlations amongst latent variables) and the Root Mean Square Error of Approximation (RMSEA – a measure of the deviation between observed covariance and that predicted by the model). Further details of these methods have previously been published (Mosley et al., 2020).

2.11. Data availability

Data analysis was performed in the R software environment (R Core Team, 2014), using the packages *FactoMineR* for PCA (Lê et al., 2008), *plspm* for PLS-PM (Sanchez, 2013) and *lavaan* for cross-lagged models (Rosseel, 2012). Pipelines for diffusion MRI processing, STN subregion and atrophy analyses can be obtained from:

https://github.com/breakspear/diffusion-pipeline.
https://github.com/AlistairPerry/DBSVATstats.
https://github.com/AlistairPerry/PDdiffusion.

A de-identified data set containing neuropsychological data can be provided by Dr Philip Mosley (Philip.Mosley@qimrberghofer.edu.au) on application, subject to institutional review board approval. Local ethics caveats and clinical privacy issues prohibit sharing of individual imaging data but a file containing AFD values can also be requested from the lead author.

3. Results

3.1. Participants

Twenty-five participants were consented and completed all assessments (Table 1). Implanted devices comprised Medtronic 3389 (n = 3), Boston Scientific Vercise ($n = 6$) and Abbott 6172 directional electrodes ($n = 16$). Current steering with directional electrodes was utilised in five participants. Stimulation parameters are reported in Supplementary Table 1. Across all participants, subthalamic VATs in each hemisphere were concatenated, with the highest probability of stimulation occurring in the dorsolateral aspect of the STN in both hemispheres but with some involvement of the medial / inferior border and dispersion of charge outside of the STN itself (Fig. 2). Summary statistics quantifying STN subregion occupancy by the simulated VAT were calculated (Supplementary Table 2). With regard to motor symptoms, there was no significant difference between preoperative UPDRS '*on*' medication and postoperative UPDRS '*on*' stimulation, but levodopa equivalent daily dose was significantly reduced ($t = 5.61$, mean reduction 786.0 mg, *corrected* $p = 9.1 \times 10^{-6}$). There was a non-significant trend associating years since diagnosis of Parkinson's disease with subcortical atrophy ($r = 0.38$, $p = 0.059$).

3.2. Cohort-level changes in initiation, inhibition and strategy use

We evaluated cohort-level changes in these measures six months after subthalamic DBS, at which time participants were stably established on stimulation (Table 1).

On the verbal fluency task, there was a significant postoperative reduction in phonemic verbal fluency ($t = 3.74$, *corrected* $p = 0.030$) but no significant group-level differences in semantic verbal fluency (*corrected* $p = 0.83$) or energization (*corrected* $p = 0.36$).

On the spontaneous speech task, there were no significant pre- to postoperative, group-level differences for both the picture description task (*corrected* $p = 0.68$ for true words generated and *corrected* $p = 0.84$ for energization ratio) and the self-generated narrative (*corrected* $p = 0.84$ for words and *corrected* $p = 0.84$ for energization).

On the Hayling test, there was a significant group-level improvement in performance post-DBS. The overall scaled score increased ($t = -3.36$, *corrected* $p = 0.013$) and this was primarily driven by a reduced global error score ($t = 3.05$, *corrected* $p = 0.013$); particularly by fewer category B errors ($t = 3.70$, *corrected* $p = 0.013$). There was a significant increase in category C responses that utilized a strategy ($t = -3.19$, *corrected* $p = 0.013$), but there was no significant change in the category A error ratio, which remained relatively high both pre- and post-DBS, indicating that strategy use reduced subtle errors but did not alter the likelihood of gross suppression failures in this cohort. Additionally, a greater suppression–initiation response time difference (suggesting strategic inefficiency) was correlated with category B errors ($r = 0.52$, *corrected* $p = 0.013$), again suggesting that a delayed response caused by the lack of a clear strategy was more likely to produce a subtle '*somewhat connected*' error rather than a blatant suppression failure.

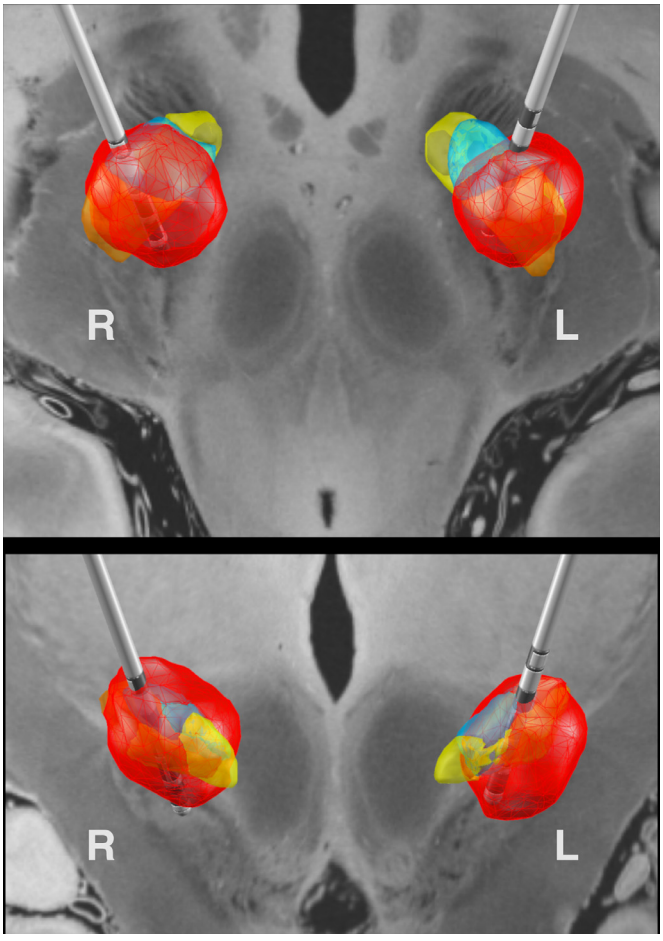

Fig. 2. Subthalamic stimulation.
Volumes of activated tissue (VATs) for each participant in each hemisphere were concatenated and thresholded to identify the highest frequency of overlapping voxels (the top 25 % are shown here). The VATs overlapped most substantially with the dorsolateral aspects of the STN in both hemispheres but included the medial / inferior aspects of the nucleus with considerable dispersion of charge outside of the STN borders. The subthalamic atlas (Ewert et al., 2018) is overlaid on a 7 Tesla MRI ex-vivo brain image (Edlow et al., 2019). Within each STN affective = yellow, associative = blue and motor = maroon subregions. Top = axial and bottom = coronal visualisations of stimulation across the whole cohort (red) with one subthalamic electrode shown for reference purposes.

On the excluded letter fluency task, there were no significant pre- to post-DBS cohort-level differences in the number of correct responses or the number of rule violations. Interestingly, the number of correct ELF responses was significantly correlated with measures of phonemic fluency ($r = 0.64$, *corrected* $p = 0.013$) and Hayling suppression response time ($r = -0.59$, *corrected* $p = 0.013$), suggesting that this measure recruited elements of both initiation and inhibition.

In the Hayling test, the category A error ratio is calculated as the number of category A errors in the last ten items relative to the total number of category A errors across all fifteen items. In the verbal fluency task, the energization ratio is calculated as the number of correct words generated in the last forty-five seconds of the task, relative to the full sixty seconds. In the spontaneous speech task, the energization ratio is calculated as the number of narrative words generated in the last forty-five seconds of the task, relative to the full sixty seconds.

Table 1
Demographic and clinical characteristics of PD cohort (n=25).

Demographic & Disease-Related Variables **Total, Percentage** **Categorical Variable** **Gender**	**Total (n = 25)** *n*	**Percentage Total** % total
Male	15	60.0
Female	10	40.0
Clinical Subtype	n	% total
Akinetic-Rigid	8	32.0
Mixed	13	52.0
Tremor	4	16.0

Continuous Variable	**Mean (SD), Median (Range)**
Age (Years)	62.5 (±10.4), 65 (38 - 77)
Hoehn & Yahr Stage	2.5 (±0.3), 2.5 (2 - 3)
Years Since Diagnosis	8.0 (±3.0), 8 (2 - 17)

Variables Assessed Pre- & Post-DBS **Mean (SD), Median (Range)** **Motor Outcomes**	**Pre-DBS**	**Post-DBS**	**Pre- vs. Post-DBS**†
Levodopa Equiv. Daily Dose	1148.0 (±653.3), 1015 (0 - 3300)	362.1 (±278.2), 300 (0 - 1175)	t = 5.61 *corr.* $p = 9.1 \times 10^{-6}$ ***
Dopamine Agonist Equiv. Daily Dose	88.2 (±108.1), 37.5 (0 - 375)	60.5 (±75.3), 37.5 (0 - 225)	t = 1.72 *corr.* p = 0.23
UPDRS Part III Motor	44.6 (±14.7), 45 (21 - 70)	40.5 (±13.0), 41 (19 - 70)	t = 1.22 *corr.* p = 0.23
Verbal Fluency	**Pre-DBS**	**Post-DBS**	**Pre- vs. Post-DBS**†
Phonemic Fluency (FAS)	57.2 (±15.5), 54 (30 - 108)	48.6 (±14.7), 48 (20 - 82)	t = 3.74 *corr.* p = 0.030 *
Semantic Fluency (Animals)	23.1 (±7.6), 22 (6 - 46)	22.8 (±6.6), 21 (12 - 39)	t = 0.22 *corr.* p = 0.83
Energization Ratio (Phonemic Fluency)	0.62 (±0.05), 0.62 (0.53 - 0.71)	0.61 (±0.08), 0.62 0.4 - 0.74)	t = 1.21 *corr.* p = 0.36
Spontaneous Speech	**Pre-DBS**	**Post-DBS**	**Pre- vs. Post-DBS**†
Picture Description Total Words	116.1 (±32.5), 114 (48 - 180)	125.4 (±41.2), 117 (60 - 229)	t = -1.40 *corr.* p = 0.68
Picture Description Energization Ratio	66.5 (±6.7), 68.9 (51.6 – 76.6)	67.0 (±13.1), 67.0 (28.3 - 88.7)	t = -0.21 *corr.* p = 0.84
Self-Generated Narrative Total Words	133.0 (±31.0), 130 (72 - 206)	134.6 (±36.2), 127 (67 - 233)	t = -0.32 *corr.* p = 0.84
Self-Generated Narrative Energization Ratio	68.6 (±7.3), 69.9 (50 - 78.6)	69.5 (±9.0), 71.6 (36.9 - 78.5)	t = -0.44 *corr.* p = 0.84
Hayling Test	**Pre-DBS**	**Post-DBS**	**Pre- vs. Post-DBS**†
Overall Scaled Score	4.9 (±1.2), 4 (3 - 7)	5.8 (±1.7), 6 (3 - 9)	t = -3.36 *corr.* p = 0.013 *
Initiation RT (secs)	5.0 (±5.4), 3 (0 - 22)	3.6 (±4.7), 2 (0 - 19)	t = 1.12 *corr.* p = 0.27
Suppression RT (secs)	23.7 (±15.2), 18 (4 - 52)	20.9 (±20.6), 10 (1 - 64)	t = 0.82 *corr.* p = 0.42
Suppression-Initiation RT Difference (secs)	18.6 (±12.9), 13 (4 - 49)	17.3 (±20.4), 8 (-8 - 63)	t = 0.35 *corr.* p = 0.79
Global Error Score	12.2 (±8.0), 15 (0 - 24)	7.9 (±7.0), 8 (0 - 20)	t = 3.05 *corr.* p = 0.013 *
All Category A Errors	2.6 (±2.0), 3 (0 - 6)	1.8 (±1.8), 2 (0 - 5)	t = 2.09 *corr.* p = 0.082
Category A Error Ratio	0.56 (±0.38), 0.67 (0 - 1)	0.43 (±0.43), 0.50 (0 - 1)	t = 1.48 *corr.* p = 0.19
All Category B Errors	4.6 (±2.8), 5 (0 - 10)	2.6 (±2.3), 2 (0 - 9)	t = 3.70 *corr.* p = 0.013 *
Category B Errors Semantic to Response	2.8 (±2.2), 3 (0 - 6)	1.8 (±1.8), 1 (0 - 6)	t = 2.67 *corr.* p = 0.026 *
Category B Errors Semantic to Subject	0.36 (±0.49), 0 (0 - 1)	0.16 (±0.37), 0 (0 - 1)	t = 1.73 *corr.* p = 0.13
Category B Semantic but Bizarre	1.4 (±1.0), 1 (0 - 3)	0.72 (±1.0), 0 (0 - 4)	t = 3.07 *corr.* p = 0.013 *
All Category C Responses	7.8 (±4.3), 7 (2 - 15)	10.6 (±3.9), 11 (5 - 17)	t = -3.33 *corr.* p = 0.013 *
Category C Responses with Strategy	3.1 (±3.6), 1 (0 - 12)	5.9 (±4.6), 6 (0 - 13)	t = -3.19 *corr.* p = 0.013 *
Category C Responses with No Obvious Strategy	4.7 (±2.8), 4 (0 - 12)	4.8 (±2.2), 5 (0 - 8)	t = -0.11 *corr.* p = 0.91
Excluded Letter Fluency	**Pre-DBS**	**Post-DBS**	**Pre- vs. Post-DBS**†
Total Correct	44.4 (±16.5), 44 (17 - 84)	40.7 (±17.2), 38 (11 - 80)	t = 2.19 *corr.* p = 0.12
Rule Violations	6.6 (±4.4), 6 (0 - 16)	6.4 (±3.4), 7 (0 - 13)	t = 0.23 *corr.* p = 0.82

† FDR-corrected per Benjamini and Hochberg (1995), with $\alpha = 0.05$.
* $p < 0.05$.
** $p < 0.01$.
*** $p < 0.001$
RT = Response Time

3.3. Principal components analysis

Both pre-and post-DBS, PCA of the neuropsychological instruments returned four dimensions (components) of initiation, inhibition and strategy use with eigenvalues of one or greater, accounting for 72.5 % (pre-DBS) and 72.4 % (post-DBS) of the total variance in the data (Table 2 and scree plots visualised in Supplementary Figs. 4 and 5). At both intervals, Dimension 1 reflected *Hayling inhibition and strategy use*, comprising the inhibitory measures Hayling category A and B total errors, global error score and suppression response time, in addition to measures of strategic efficiency including the initiation–suppression response time difference and the number of strategic category C responses. Dimension 2 reflected *initiation*, with a similar composition of instruments at both intervals. Prior to DBS, Dimension 2 incorporated phonemic fluency, the phonemic energization ratio and the total number of words generated in the self-generated narrative. Postoperatively, Dimension 2 also included the total number of correct responses in the ELF task and the total number of words generated in the picture description task, but not the phonemic energization ratio. Dimension 3 also reflected *initiation* but with a greater emphasis on energization ratios than compared to Dimension 2, being formed preoperatively from the energization ratios for both spontaneous speech tasks and the total number of words in the picture description task. Postoperatively, Dimension 3 was made up from the phonemic and picture description energization ratios and the total number of words in both spontaneous speech tasks. Finally, Dimension 4 predominantly reflected *inhibition,* with ELF rule violations making the largest contribution both pre- and post-DBS. The Hayling category A error ratio (blatant errors through the 15 items) and the Hayling initiation response time were also represented at both intervals. Notably, prior to DBS, ELF rule violations and the Hayling category A error ratio were correlated positively on Dimension 4, whilst postoperatively they were correlated negatively. This particular combination of measures suggests a '*task-setting*' component to this dimension, reflecting an inability to obtain task rules and apply them consistently to avoid error.

The broad alignment of these dimensions pre- and post-DBS indicated that the expression of initiation and inhibition remained similar at both timepoints in this cohort. The separation of inhibitory measures on the Hayling and ELF tasks suggested that these instruments assessed different components of inhibition, whilst the greater contribution of energization ratios in Dimension 3 as compared to Dimension 2 suggested a different representation of initiation.

3.4. Structural connectivity, subthalamic stimulation and individual variability

We were interested in whether individual differences in initiation, inhibition and strategy use were related to the structural connectivity of a frontal network linked to the STN, as well as whether postoperative variability in these cognitive operations was linked to the effects of stimulation on this network. In order to discriminate the influence of specific cortical areas and their connectivity, we reported individual weights for each tract in the PLS path model in order to characterise key tracts for each construct. We simulated the volume of activated tissue (VAT) for each participant, based on individualised stimulation parameters after six postoperative months, following reconstruction of the electrode trajectory and identification of the locus of subthalamic stimulation in each hemisphere. We reconstructed the structural connectivity of the field of stimulation within the frontal network, with the subthalamic VAT replacing the STN as the network hub. Both pre- and postoperatively, we assessed whether variability was also mediated by differences in dopaminergic medication, age, years since diagnosis of Parkinson's disease or a subcortical atrophy score. Post-DBS, we incorporated estimates of local stimulation diffusion within motor, cognitive-associative and affective subregions of the STN, in order to assess the relative contribution of focal stimulation within the target nucleus. Finally, we evaluated whether the baseline connectivity of cortico-STN fibres also had an influence on pre- to postoperative changes in these executive functions.

3.4.1. Dimension 1 (Hayling inhibition and strategy use)

We first examined individual differences in Dimension 1, which comprised measures of inhibition and strategic efficiency from the Hayling test. These constructs were significantly related to prefrontal cortico-subthalamic connectivity at baseline. Prior to DBS, the greater the structural connectivity of the STN with the prefrontal network, the fewer the inhibitory errors, the faster the response time in the suppression condition and the greater the use of strategy (coefficient = -0.77, $p = 1.6 \times 10^{-4}$, Table 3), with tracts connecting the STN with the IFG and SMA in the right hemisphere weighted strongly in this model (Fig. 3 and Supplementary Table 3).

Six months after STN-DBS, we modelled the connectivity of networks incorporating the participant-specific stimulation field at each DBS electrode. Similar to the preoperative interval, the greater the structural connectivity of the VAT with the prefrontal network, the fewer the inhibitory errors, the faster the response time in the suppression condition and the greater the use of strategy (coefficient = -0.59, $p = 0.016$, Table 4), with tracts connecting the VAT with the OFC in both hemispheres weighted strongly in this model (Fig. 3 and Supplementary Table 3). There was no significant effect of regional STN stimulation ($p = 0.20$).

We used two methods to evaluate whether postoperative inhibition and strategy use was related to the pre-surgical structure and connectivity of the brain. Firstly, we calculated the participant-wise atrophy in a subcortical network identified as a potential vulnerability marker for the cortical spread of neurodegeneration in Parkinson's disease. For Dimension 1, there was no significant effect of subcortical atrophy ($p = 0.36$) on postoperative variability in this domain. Secondly, we used a cross-lagged model to assess whether baseline cortico-STN connectivity strength in key tracts was a significant determinant of pre-to postoperative impairment in inhibition and strategy use. For Dimension 1, the connectivity of the OFC with the site of stimulation in both hemispheres most significantly influenced postoperative variability in this component of executive functioning – therefore we examined the baseline connectivity of the STN with these prefrontal regions. Greater connectivity of the STN with both right and left OFC prior to DBS was associated with superior inhibition and strategy use after DBS (right STN-OFC coefficient = -0.21, $p = 0.0010$; left STN-OFC coefficient = -0.22, $p = 0.012$, Table 5).

3.4.2. Dimension 2 (Initiation)

We then assessed individual differences in Dimension 2, which was formed from measures of initiation. At baseline, the greater the connectivity of the STN with the prefrontal network, the greater the effectiveness of initiation, manifest with greater phonemic fluency, a sustained ability to generate words beginning with the specified letter across sixty seconds and a higher total number of words generated in narrative speech (coefficient = 0.93, $p = 7.4 \times 10^{-10}$, Table 3). Tracts connecting the STN with the IFG in the right hemisphere and the STN with the vmPFC and OFC in the left hemisphere were weighted strongly (Fig. 4 and Supplementary Table 4).

Postoperatively, again greater connectivity of the VAT with the prefrontal network was associated with more effective initiation, manifest with greater phonemic fluency, a higher total number of words generated in both narrative and descriptive speech, as well as a greater number of correct responses on the ELF task (coefficient = 0.62, $p = 2.9 \times 10^{-4}$, Table 4), with tracts connecting the VAT with the IFG and OFC in the left hemisphere weighted strongly (Fig. 4 and Supplementary Table 4). There was also a significant positive effect of regional STN stimulation on postoperative initiation (coefficient = 0.35, $p = 0.026$, Table 4), with the right motor STN subregion weighted most strongly.

For Dimension 2, there was no significant effect of subcortical atrophy ($p = 0.070$) on postoperative variability in this domain.

Table 2
Principal components analysis of neuropsychological instruments.

Pre-DBS Measure	Representation	Dimension 1 Eigenvalue = 4.76	Dimension 2 Eigenvalue = 3.94	Dimension 3 Eigenvalue = 2.16	Dimension 4 Eigenvalue = 1.46
Phonemic Fluency (FAS)	*Contribution*	-	11.2 %	-	-
	Correlation	-	0.66	-	-
Semantic Fluency (Animals)	*Contribution*	-	-	-	-
	Correlation	-	-	-	-
Energization Ratio (Phonemic Fluency)	*Contribution*	-	10.2 %	-	14.1 %
	Correlation	-	0.64	-	0.45
Picture Description Total Words	*Contribution*	-	-	17.7 %	-
	Correlation	-	-	0.62	-
Picture Description Energization Ratio	*Contribution*	-	-	18.9 %	-
	Correlation	-	-	0.64	-
Self-Generated Narrative Total Words	*Contribution*	-	15.4 %	-	-
	Correlation	-	0.78	-	-
Self-Generated Narrative Energization Ratio	*Contribution*	-	-	20.8 %	-
	Correlation	-	-	0.67	-
Hayling Initiation RT	*Contribution*	-	-	-	21.4 %
	Correlation	-	-	-	0.56
Hayling Suppression RT	*Contribution*	13.2 %	-	-	-
	Correlation	0.79	-	-	-
Hayling Suppression-Initiation RT Difference	*Contribution*	13.0 %	-	-	-
	Correlation	0.79	-	-	-
Haying Category A Errors	*Contribution*	10.3 %	-	-	-
	Correlation	0.70	-	-	-
Hayling Category B Errors	*Contribution*	12.1 %	-	-	-
	Correlation	0.76	-	-	-
Hayling Global Error Score	*Contribution*	13.1 %	-	-	-
	Correlation	0.79	-	-	-
Hayling Category A Error Ratio	*Contribution*	-	-	-	10.9 %
	Correlation	-	-	-	-
Hayling Inverse Category C Responses with Strategy	*Contribution*	8.8 %	-	-	-
	Correlation	0.64	-	-	-
ELF Total Correct	*Contribution*	-	-	-	-
	Correlation	-	-	-	-
ELF Rule Violations	*Contribution*	-	-	-	39.9 %
	Correlation	-	-	-	0.76
Post-DBS Measure	Representation	Dimension 1 Eigenvalue = 5.09	Dimension 2 Eigenvalue = 3.96	Dimension 3 Eigenvalue = 1.72	Dimension 4 Eigenvalue = 1.55
Phonemic Fluency (FAS)	*Contribution*	-	9.8 %	-	-
	Correlation	-	0.62	-	-
Semantic Fluency (Animals)	*Contribution*	-	-	-	-
	Correlation	-	-	-	-
Energization Ratio (Phonemic Fluency)	*Contribution*	-	-	16.0 %	-
	Correlation	-	-	0.52	-
Picture Description Total Words	*Contribution*	-	13.4 %	19.2 %	-
	Correlation	-	0.73	0.57	-
Picture Description Energization Ratio	*Contribution*	-	-	20.4 %	-
	Correlation	-	-	0.59	-
Self-Generated Narrative Total Words	*Contribution*	-	11.3 %	13.3 %	-
	Correlation	-	0.67	0.48	-
Self-Generated Narrative Energization Ratio	*Contribution*	-	-	-	15.2 %
	Correlation	-	-	-	0.49
Hayling Initiation RT	*Contribution*	-	-	-	15.4 %
	Correlation	-	-	-	0.49
Hayling Suppression RT	*Contribution*	14.6 %	-	-	-
	Correlation	0.86	-	-	-
Hayling Suppression-Initiation RT Difference	*Contribution*	13.5 %	-	-	-
	Correlation	0.83	-	-	-
Haying Category A Errors	*Contribution*	9.3 %	-	-	-
	Correlation	0.69	-	-	-
Hayling Category B Errors	*Contribution*	11.1 %	-	-	-
	Correlation	0.75	-	-	-
Hayling Global Error Score	*Contribution*	12.1 %	-	-	-
	Correlation	0.79	-	-	-
Hayling Category A Error Ratio	*Contribution*	-	-	-	15.5 %
	Correlation	-	-	-	-0.49
Hayling Inverse Category C Responses with Strategy	*Contribution*	11.5 %	-	-	-
	Correlation	0.77	-	-	-
ELF Total Correct	*Contribution*	-	13.3 %	-	-
	Correlation	-	0.73	-	-
ELF Rule Violations	*Contribution*	-	-	-	21.4 %
	Correlation	-	-	-	-0.58

Table 3
Modelling the effect of structural connectivity on initiation, inhibition & strategy use prior to STN-DBS.

PLS-PM Analysis of Dimensions 1-4 Prior to STN-DBS Dimension	Heavily-Weighted Tracts in Network	R^2	Path Coefficient	Significance	95 % C.I.	Other Significant Co-variates
1	Right STN-IFG (0.85) Right STN-SMA (0.66)	0.69	-0.77	$p = 1.7 \times 10^{-4}$ ***	-1.31 – -0.48	Nil
2	Right STN-IFG (0.71) Left STN-OFC (0.59) Left STN-vmPFC (0.56)	0.88	0.93	$p = 7.4 \times 10^{-10}$ ***	0.83 – 1.05	Nil
3	Right STN-vmPFC (1.45) Left STN-ACC (0.98)	0.64	-0.70	$p = 5.2 \times 10^{-4}$ ***	-0.91 – -0.32	Nil
4	Left STN-vmPFC (1.03) Left STN-SMA (0.96) Left STN-OFC (0.61)	0.61	-0.63	4.5×10^{-4} ***	-0.88 – -0.19	i) Atrophy *coeff* = -0.34 95 % CI = -0.66 – 0.41 $p = 0.042$ * ii) Atrophy x Connectivity *coeff* = -0.33 95 % CI = -1.04 – 0.27 $p = 0.039$ *

* $p < 0.05$.
** $p < 0.01$.
*** $p < 0.001$
ACC = anterior cingulate cortex, IFG = inferior frontal gyrus, OFC = orbitofrontal cortex, SMA = pre-supplementary motor area, STN = subthalamic nucleus, vmPFC = ventromedial prefrontal cortex.

Table 4
Modelling the effect of structural connectivity & local subthalamic stimulation on initiation, inhibition & strategy use after STN-DBS.

PLS-PM Analysis of Dimensions 1-4 Subsequent to STN-DBS Dimension	Heavily-Weighted Tracts in Network	R^2	Path Coefficient	Significance	95 % C.I.	Other Significant Co-variates
1	Right VAT-OFC (0.59) Left VAT-OFC (0.94)	0.71	-0.59	$p = 0.016$ *	-1.04 – -0.075	Nil
2	Left VAT-IFG (1.06) Left VAT-OFC (0.70)	0.72	0.62	$p = 2.9 \times 10^{-4}$ ***	0.38 – 0.89	i) Focal STN Stimulation *coeff* = 0.35 95 % CI = -0.057 – 0.66 $p = 0.026$ Heavily Weighted STN Subregions: Right Motor (0.65)
3	Right VAT-IFG (1.10) Left VAT-OFC (0.68)	0.52	-0.44	$p = 0.048$ *	-1.07 – 0.097	Nil
4	Right VAT-IFG (1.08) Right VAT-OFC (0.98)	0.66	-0.71	$p = 0.0010$ **	-1.03 – -0.27	Nil

* $p < 0.05$.
** $p < 0.01$.
*** $p < 0.001$
ACC = anterior cingulate cortex, IFG = inferior frontal gyrus, OFC = orbitofrontal cortex, SMA = pre-supplementary motor area, VAT = volume of activated tissue, vmPFC = ventromedial prefrontal cortex.

Cross-lagged models were tested for tracts connecting the STN with the OFC and IFG in the left hemisphere, as the connectivity of these cortical regions with the site of stimulation were identified as key mediators of variability in postoperative initiation. However, neither the baseline connectivity of the STN-IFG ($p = 0.49$) nor the STN-OFC ($p = 0.63$) influenced pre- to postoperative change in the effectiveness of initiation (Table 5).

3.4.3. Dimension 3 (Initiation)

Individual variability in Dimension 3 comprised strong contributions from energization ratios and spontaneous speech production both pre- and post-DBS. Prior to DBS, in contrast to Dimension 2, the greater the connectivity of the STN with the prefrontal network, the less efficient was initiation, with reduced spontaneous speech production and a lesser capacity to sustain verbal responding across sixty seconds

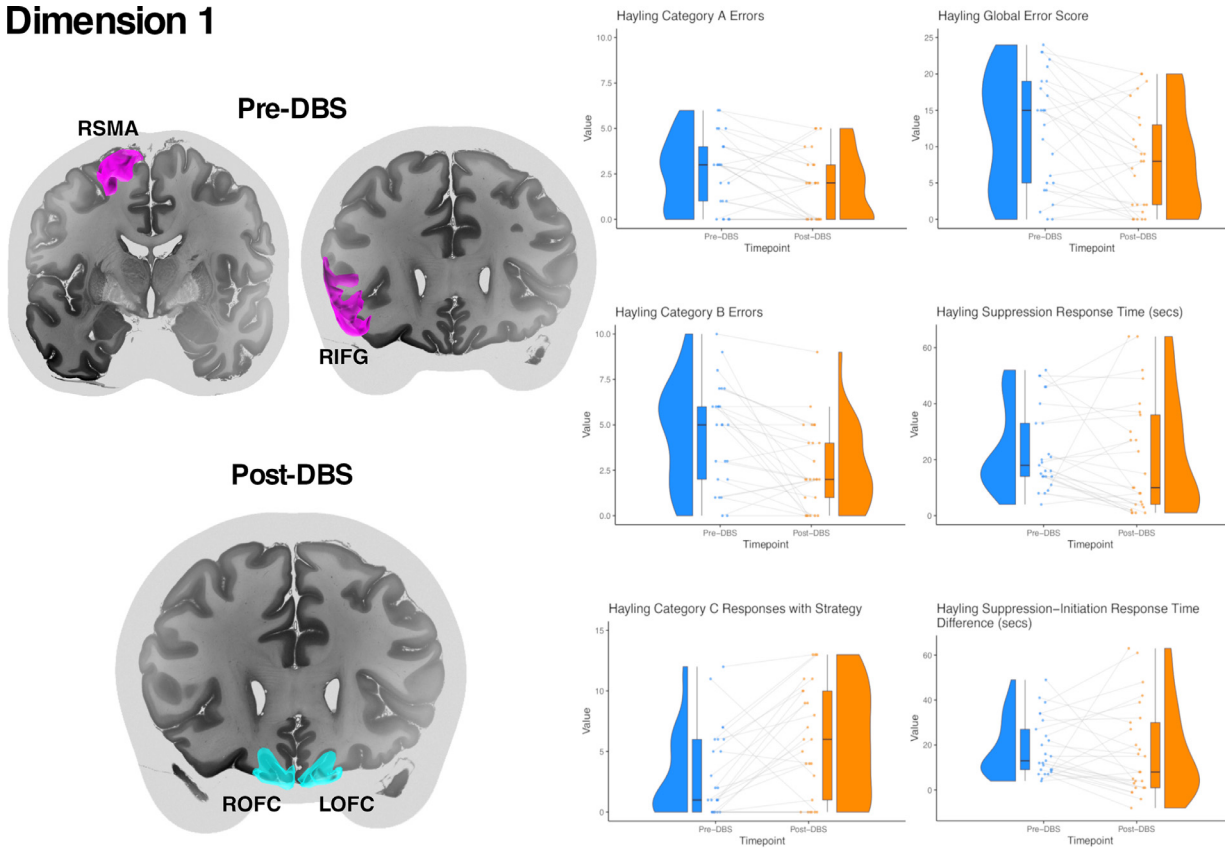

Fig. 3. Dimension 1 (Hayling Inhibition & Strategy Use).
Left Panel: Prior to DBS, the greater the structural connectivity of the STN with the right IFG and SMA, the fewer the inhibitory errors on the Hayling test, and the greater the use of strategy. Postoperatively, the greater the connectivity of the VAT with the OFC in both hemispheres, the fewer the inhibitory errors, and the greater the use of strategy. Cortical regions are overlaid upon a 7-Tesla MRI at 100 micron resolution (Edlow et al., 2019). Right Panel: Dimension 1 comprised measures of inhibition and strategic efficiency from the Hayling test. Raincloud plots made with code provided by Allen et al. (2019) and van Langen (2020).
IFG = inferior frontal gyrus, OFC = orbitofrontal cortex, SMA = pre-supplementary motor area, STN = subthalamic nucleus, VAT = volume of activated tissue.

Table 5
Modelling the effect of baseline subthalamic connectivity on initiation, inhibition & strategy use after STN-DBS.

Cross-Lagged Model Results						
	Cross-Lagged Coefficients		**Cross-Sectional Coefficients**		**Model Fit Indices**	
Dimension & Tract	$Connectivity_{t1}$ → $\Delta Behaviour$	$Behaviour_{t1}$ → $\Delta Connectivity$	$Connectivity_{t1}$ ~ $Behaviour_{t1}$	$\Delta Connectivity$ ~ $\Delta Behaviour$	**CFI**	**RMSEA**
1	*coeff* = -0.21	*coeff* = -0.29	*coeff* = -2.26	*coeff* = -1.12	1.0	0.001
Right STN-OFC	p = 0.0010 **	p = 0.034 *	p = 0.013 *	p = 0.086		
1	*coeff* = -0.22	*coeff* = -0.18	*coeff* = -1.00	*coeff* = 0.00	1.0	0.001
Left STN-OFC	p = 0.012 *	p = 0.12	p = 0.37	p = 1.00		
2	*coeff* = 0.074	*coeff* = 0.38	*coeff* = 0.98	*coeff* = -0.069	1.0	0.001
Left STN-IFG	p = 0.49	p = 0.046 *	p = 0.36	p = 0.83		
2	*coeff* = -0.048	*coeff* = -0.44	*coeff* = 3.49	*coeff* = 1.18	1.0	0.001
Left STN-OFC	p = 0.63	p = 0.062	p = 0.022 *	p = 0.10		
3	*coeff* = 0.056	*coeff* = -0.39	*coeff* = -1.12	*coeff* = -0.49	1.0	0.001
Right STN-IFG	p = 0.39	p = 0.26	p = 0.16	p = 0.52		
3	*coeff* = 0.042	*coeff* = -0.27	*coeff* = -1.26	*coeff* = -0.33	1.0	0.001
Left STN-OFC	p = 0.42	p = 0.47	p = 0.14	p = 0.43		
4	*coeff* = -0.054	*coeff* = -0.25	*coeff* = -0.17	*coeff* = -0.27	1.0	0.001
Right STN-IFG	p = 0.44	p = 0.63	p = 0.75	p = 0.66		
4	*coeff* = -0.17	*coeff* = -0.045	*coeff* = -1.30	*coeff* = -0.36	1.0	0.001
Right STN-OFC	p = 0.65	p = 0.40	p = 0.22	p = 0.54		

Significance:
* $p < 0.05$.
** $p < 0.01$.
*** $p < 0.001$

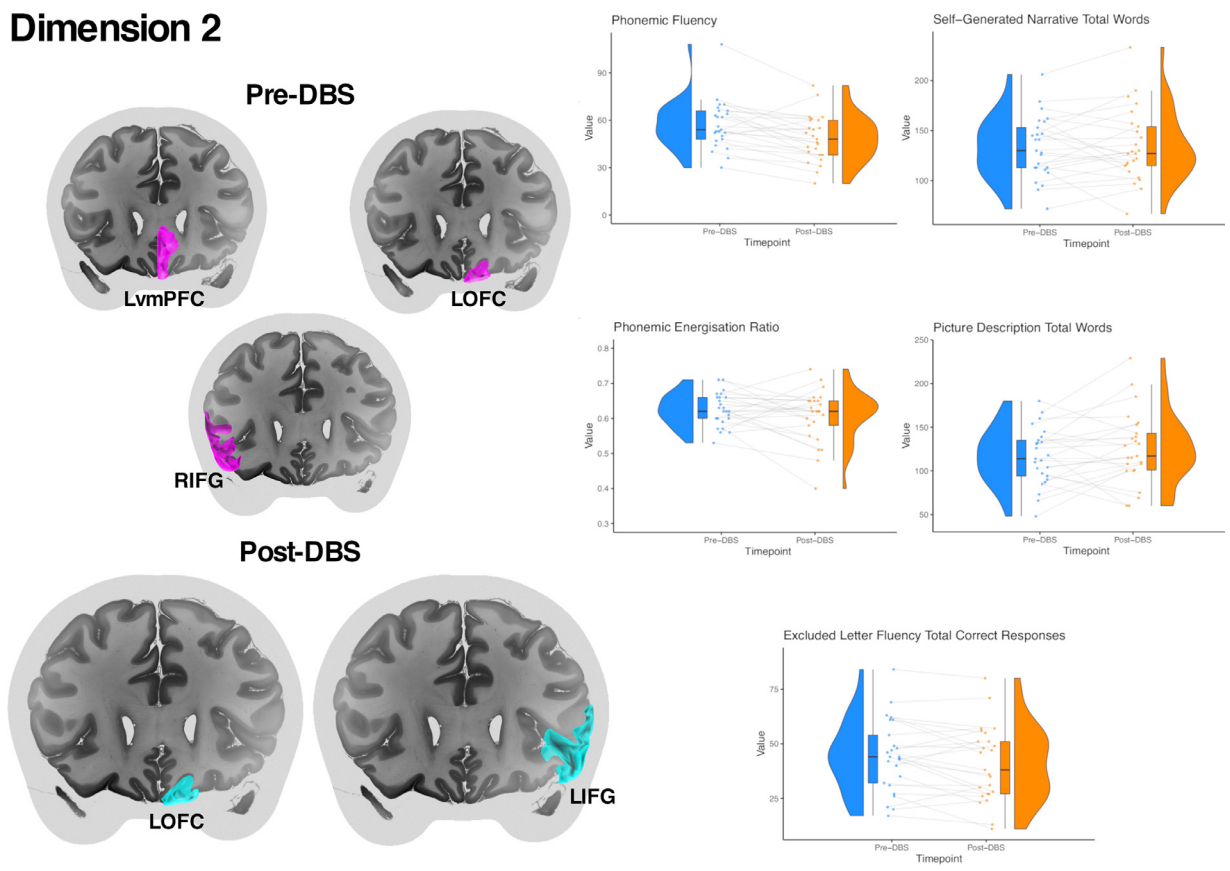

Fig. 4. Dimension 2 (Initiation).
Left Panel: Prior to DBS, the greater the structural connectivity of the STN with the right IFG, left vmPFC and left OFC, the greater the effectiveness of initiation, manifest with greater phonemic fluency, sustained phonemic energization and greater spontaneous speech production. Postoperatively, the greater the connectivity of the VAT with the left IFG and OFC, the greater the phonemic fluency, spontaneous speech production and correct responses on the ELF task. Cortical regions are overlaid upon a 7-Tesla MRI at 100 micron resolution (Edlow et al., 2019). Right Panel: Dimension 2 comprised measures of initiation including phonemic fluency, the phonemic energization ratio, spontaneous narrative and descriptive speech, as well as correct responses on the ELF task. Raincloud plots made with code provided by Allen et al. (2019) and van Langen (2020).
ELF = excluded letter fluency, IFG = inferior frontal gyrus, OFC = orbitofrontal cortex, STN = subthalamic nucleus, VAT = volume of activated tissue, vmPFC = ventromedial prefrontal cortex.

(coefficient = -0.70, $p = 5.2 \times 10^{-4}$, Table 3). Tracts connecting the STN with the vmPFC in the right hemisphere and the STN with the ACC in the left hemisphere were weighted strongly (Fig. 5 and Supplementary Table 5).

Postoperatively, greater connectivity of the VAT with the prefrontal network was again associated with less effective initiation (coefficient = -0.44, $p = 0.048$, Table 4), with tracts connecting the VAT with the IFG in the right hemisphere and the VAT with the OFC in the left hemisphere weighted strongly (Fig. 5 and Supplementary Table 5). However, confidence intervals crossed zero for this association.

Subcortical atrophy did not significantly affect postoperative variability in Dimension 3 ($p = 0.26$). As the most strongly weighted tracts in the postoperative model, cross-lagged models were tested for the connectivity of the STN-IFG in the right hemisphere and the STN-OFC in the left hemisphere. Neither the baseline connectivity of the STN-IFG ($p = 0.39$) nor the STN-OFC ($p = 0.42$) influenced pre- to postoperative change in disinhibition (Table 5).

3.4.4. *Dimension 4 (Inhibition)*

Finally, we studied inter-individual variability in Dimension 4, which was predominantly composed of rule violations in the ELF task, with additional contributions from the Hayling category A error ratio and measures of initiation derived from the Hayling test and verbal tasks. Preoperatively, the greater the connectivity of the STN with the prefrontal network, the greater the effectiveness of inhibition, manifest with fewer rule violations and fewer blatant suppression errors resulting from a lack of a strategy (coefficient = -0.63, $p = 4.5 \times 10^{-4}$, Table 3). Tracts connecting the STN with the OFC, SMA and vmPFC in the left hemisphere were weighted strongly (Fig. 6 and Supplementary Table 6). There was also a significant association between subcortical atrophy and Dimension 4, with preserved subcortical volume also associated with greater inhibition (coefficient = -0.34, $p = 0.042$) and a greater interaction effect of subcortical volume x connectivity associated with greater inhibition (coefficient = -0.33, $p = 0.039$). However, confidence intervals were wide for both of these metrics and crossed zero (Table 3).

Six months after STN-DBS, the greater the connectivity of the site of stimulation with the prefrontal network, the greater the disinhibition (note the negative correlations on the PCA for Dimension 4) with more ELF rule violations and more blatant suppression errors resulting from a lack of strategy (coefficient = -0.71, $p = 0.0010$, Table 4), with tracts connecting the VAT with the IFG and OFC in the right hemisphere weighted strongly (Fig. 6 and Supplementary Table 6).

There was no significant effect of subcortical atrophy ($p = 0.28$) on postoperative variability in this Dimension 4. Cross lagged models were tested for tracts connecting the STN with the OFC and IFG in the right hemisphere. Neither the baseline connectivity of the STN-IFG ($p = 0.44$) nor the STN-OFC ($p = 0.65$) influenced pre- to postoperative change in disinhibition (Table 5).

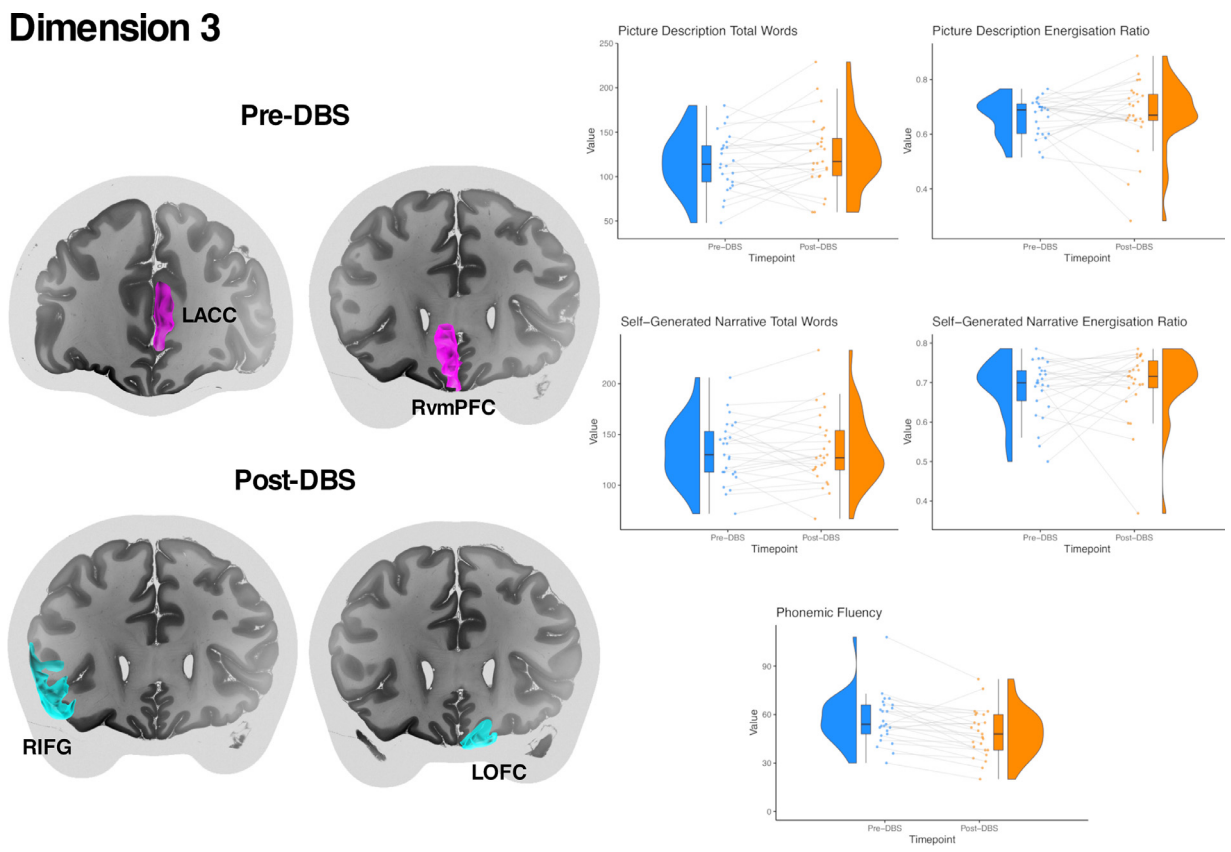

Fig. 5. Dimension 3 (Initiation).
Left Panel: Prior to DBS, the greater the structural connectivity of the STN with the right vmPFC and left ACC, the less efficient was initiation, manifest with reduced descriptive speech and a reduced energization ratio for descriptive and narrative speech. Postoperatively, the greater the connectivity of the VAT with the right IFG and left OFC, the lesser was narrative and descriptive speech production and the lesser was the energization ratio for descriptive speech and phonemic fluency. Cortical regions are overlaid upon a 7-Tesla MRI at 100 micron resolution (Edlow et al., 2019). Right Panel: Dimension 3 comprised measures of initiation including spontaneous narrative and descriptive speech, energization ratios for both these measures and the phonemic energization ratio. Raincloud plots made with code provided by Allen et al. (2019) and van Langen (2020).
ACC = anterior cingulate cortex, IFG = inferior frontal gyrus, OFC = orbitofrontal cortex, STN = subthalamic nucleus, VAT = volume of activated tissue, vmPFC = ventromedial prefrontal cortex.

3.5. Supplementary analyses

Given the correlation of strategic inefficiency with category B (subtle) but not category A (blatant) suppression errors, we examined the structural correlations with strategy use (reflected by reduced suppression-initiation response time difference, reduced Hayling category A error ratio and increased Hayling category C responses resulting from the use of a strategy). Preoperatively, strategy use was significantly associated with a prefrontal network in which the right STN-IFG and right STN-SMA tracts were weighted most heavily, with stronger connectivity associated with greater strategy use (coefficient = -0.78, $p = 9.2 \times 10^{-5}$, Supplementary Table 7).

Postoperatively, stronger connectivity of the subthalamic VAT with the prefrontal network was also associated with greater strategy use (coefficient = -0.67, $p = 0.0033$, Supplementary Table 5) but in this model, connectivity of the VAT with the OFC in both hemispheres was weighted strongly. There was no significance of focal STN stimulation ($p = 0.74$) or subcortical atrophy ($p = 0.14$). In the cross-lagged model, greater right (coefficient = -0.11, $p = 0.001$) and left (coefficient = -0.13, $p = 0.001$) STN-OFC connectivity at baseline was associated with a reduced pre- to postoperative change in strategy use.

In the cross-lagged model:

(i) $Connectivity_{t1} \rightarrow \Delta Behaviour$ represents connectivity to behaviour coupling: the extent to which structural connectivity at baseline associates with change in neuropsychological measures at follow up.

(ii) $Behaviour_{t1} \rightarrow \Delta Connectivity$ represents behaviour to connectivity coupling: the degree of change in structural connectivity dependent on executive functioning at baseline.

(iii) $Connectivity_{t1} \sim Behaviour_{t1}$ is connectivity-behaviour co-variance at baseline

(iv) $\Delta Connectivity \sim \Delta Behaviour$ is an estimate of correlated change: reflecting the degree to which connectivity and behaviour changes co-occur.

CFI = Comparative Fit Index, RMSEA = Root Mean Square Error of Approximation

4. Discussion

In persons with Parkinson's disease prior to subthalamic DBS, we found significant co-variation in initiation, inhibition and strategy use with the structural connectivity of a prefrontal cortical network associated with the STN. After surgery, we found that the structural connectivity of this network with a simulated volume of activated tissue also co-varied with these same executive functions. We employed a multivariate model controlling for important covariates such as age, years since diagnosis of Parkinson's disease, dopaminergic medication dosage (including the proportion of the dose composed from dopamine agonist medication), subcortical atrophy and focal stimulation effects.

We employed a range of neuropsychological tests to assess these constructs. At the level of individual instruments, we were able to

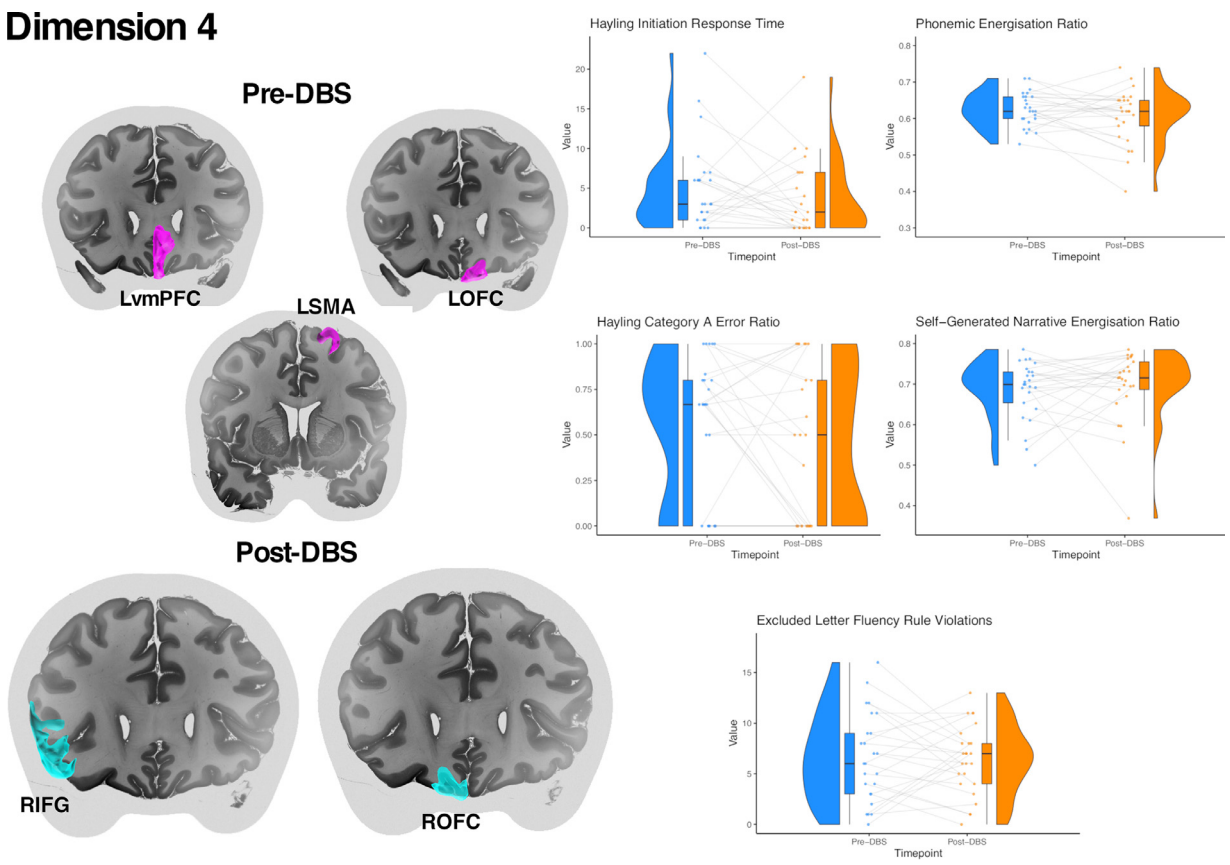

Fig. 6. Dimension 4 (Inhibition).
Left Panel: Prior to DBS, the greater the structural connectivity of the STN with the vmPFC, OFC and SMA in the left hemisphere, the fewer the rule violations and blatant suppression errors resulting from a lack of strategy. Postoperatively, the greater the connectivity of the VAT with the IFG and OFC in the right hemisphere, the greater the disinhibition, with more rule violations and blatant suppression errors. Cortical regions are overlaid upon a 7-Tesla MRI at 100 micron resolution (Edlow et al., 2019). Right Panel: Dimension 4 comprised measures of inhibition including ELF rule violations and the Hayling Category A error ratio. Together with the Hayling Initiation response time, these measures could also be seen as reflecting a '*task setting*' component – i.e. getting into '*set*' to respond appropriately on the task. Raincloud plots made with code provided by Allen et al. (2019) and van Langen (2020).
ELF = excluded letter fluency, IFG = inferior frontal gyrus, OFC = orbitofrontal cortex, SMA = pre-supplementary motor area, STN = subthalamic nucleus, VAT = volume of activated tissue, vmPFC = ventromedial prefrontal cortex.

reproduce some interesting findings from prior work using the Hayling test (Robinson et al., 2015a), such as the association between strategic inefficiency, slowed responding in the suppression condition and category B (subtle) but not A (blatant) suppression errors, both at baseline and longitudinally, where increased strategy use was associated with fewer category B (but not A) errors at six months. We also reproduced the finding of a reduction in phonemic verbal fluency after STN-DBS (Parsons et al., 2006; Witt et al., 2008; Combs et al., 2015).

The principal components analysis of the neuropsychological instruments identified four distinct dimensions that were strikingly similar pre- and post-DBS. Although these reflect different aspects of initiation, inhibition and strategy use, they retain a synergistic relationship under the general construct of '*starting and stopping*' and therefore prefrontal cortical regions classically implicated in these functions (such as the OFC and IFG) were widely implicated in the connectivity analyses. However, we replicated hemispheric distinctions reported in prior work, including a role for the right inferior frontal gyrus in inhibition and strategy use, as well as the left inferior frontal gyrus in tasks requiring selection under conditions of maintained inhibition. Postoperatively, greater connectivity of the stimulation field with right anterior cortical regions was associated with greater rule violations and suppression errors, supporting prior work implicating right-hemispheric STN stimulation in disinhibition.

Dimension 1 comprised measures of inhibition and strategy use on the Hayling test, with greater subthalamic connectivity with the IFG and SMA in the right hemisphere associated with superior performance on these measures prior to DBS. These results complement prior work undertaken in lesioned cohorts (Volle et al., 2012; Robinson et al., 2015a), as well as VBM analyses in persons with Parkinson's disease (O'Callaghan et al., 2013a). When we specifically examined strategy use in a supplementary analysis, the right IFG and SMA again emerged as key cortical regions. These findings are noteworthy in light of prior reports that the right IFG (and not other anterior regions such as the OFC) is specifically linked to strategy use on this instrument (Cipolotti et al., 2016). Yet, after STN-DBS, connectivity of the stimulation field with both left and right OFC emerged as key mediators of performance in these domains, with greater connectivity associated with greater inhibition and strategy use. These findings are atypical not only because they again implicate the OFC, but also because they suggest an enhancement in executive functioning after STN-DBS, when stimulation of the associative and affective subregions of the STN has classically been associated with impulsivity and disinhibition (Romito et al., 2002; Daniele et al., 2003; Hershey et al., 2004; Voon et al., 2006; Appleby et al., 2007; Mallet et al., 2007; Hershey et al., 2010; Welter et al., 2014; Mosley et al., 2018a). However, two findings suggest that this is not a direct stimulation effect and may instead reflect greater integrity of cortico-subthalamic afferents at baseline. First, there is no association with focal STN subregion stimulation and these findings. Second, the greater the strength of these orbitofrontal tracts prior to DBS, the less likely was pre- to postoperative impairment in these

domains, including both Dimension 1 and strategy use in isolation. In other words, this unexpected finding may not be a direct effect of stimulation *per se*, but a consequence of lesser mesolimbic degeneration in those participants with greater connectivity at baseline. Prior work has demonstrated that the extent of degeneration in prefrontal networks is variable but may be present from the early stages of Parkinson's disease (Rae et al., 2012; van der Vegt et al., 2013). Direct projections from OFC to STN are implicated in the limbic hyperdirect pathway, which provides an important inhibitory influence on affective and cognitive output from the basal ganglia (Haber and Knutson, 2010; Volkmann et al., 2010; Haynes and Haber, 2013). Progressive cortical thinning in the OFC has been demonstrated longitudinally and this region may therefore be a sensitive marker of emergent prefrontal cortical degeneration, hypothesised to be linked to strong structural connectivity with the subcortical disease reservoir propagating toxic alpha-synuclein (Yau et al., 2018). Individuals with preserved OFC-STN connectivity preoperatively may therefore have a greater anatomical substrate of '*inhibitory reserve*' that could mitigate the effects of stimulation. This underscores the value of our approach quantifying the influence of preoperative connectivity on postoperative behaviour (Table 5) because it allows this hypothesis to be tested. Future work may seek to extend these findings by testing participants '*on*' and '*off*' stimulation, as well as at different stimulation intensities, to clarify whether there is a direct contribution of stimulation and whether a biological gradient exists between stimulation and behaviour.

Dimension 2 was composed from measures of initiation, with greater subthalamic connectivity with anterior regions including the IFG, OFC and vmPFC associated with greater performance in this domain at baseline. The key role of connectivity between the field of stimulation and the left IFG after STN-DBS is significant due to the representation of phonemic fluency and correct responses on the ELF task on Dimension 2. Prior lesion work has identified a clear role of the left IFG in fluency tasks requiring selection (Robinson et al., 2010, 2012) consistent with this region mediating selection under conditions of maintained inhibition. Grey matter atrophy of the left IFG and OFC has also previously been associated with impaired ELF performance in persons with Parkinson's disease (O'Callaghan et al., 2013b). A significant effect of focal stimulation in the right motor STN subregion on improved postoperative initiation was also found. The site of this effect in the right hemisphere and in a region of the STN unlikely to have significant connectivity with these prefrontal regions suggests this is an independent effect.

Dimension 3 also reflected measures of initiation, but with a greater emphasis on energization ratios (the ability to maintain a consistent response over time). Curiously, the greater the connectivity of the STN and the stimulation field with anterior prefrontal regions, the greater the impairment in these domains both pre- and post-DBS (although noting that postoperatively this finding only just reaches the threshold for statistical significance and the confidence intervals cross zero). This isolated finding of increased connectivity associating with neuropsychological impairment may be related to the complex nature of propositional speech, which recruits many areas outside of the prefrontal cortex, including posterior parietal and middle temporal regions (Braun et al., 2001; Blank et al., 2002). It is possible that subthalamic connectivity suppresses conceptual preparation and output for these types of tasks, which are complex and require an interplay between initiation, inhibition and semantics.

Finally, Dimension 4 was made up primarily from ELF rule violations and blatant suppression errors on the Hayling task related to a lack of strategic responding. Together with the Hayling Initiation response time, these measures could also be seen as reflecting a '*task setting*' component – i.e. getting into '*set*' to respond appropriately on the task. Prior to DBS, greater left-hemispheric subthalamic connectivity was associated with increased inhibition, but postoperatively, greater connectivity of the stimulation field with the right IFG and OFC was associated with disinhibition, manifest with more rule violations and suppression errors. This complements prior work (in a non-overlapping cohort) where stimulation of the right associative STN was associated with greater postoperative disinhibition (Mosley et al., 2018b). Although no focal stimulation effects were seen on this occasion, these cortical regions (particularly the IFG) are likely to project to the associative region of the STN and support a model in which right hemispheric associative STN stimulation is more likely to induce disinhibition of this manner. Interestingly, this pre- to postoperative dissociation between the left and right hemispheres may reflect a dissociation between the top-down control of task set (left hemisphere) and impaired inhibition of inappropriate responses (right hemisphere) (Aron et al., 2004a).

We did not find a strong association between energization and the superior medial cortical regions such as the SMA, as has been previously reported in lesioned populations (Robinson et al., 2012). Aside from the divergent nature of the aetiology underlying the energization impairment in Parkinson's disease (namely dopaminergic depletion and neurodegeneration), we note that the superior medial region defined in this prior lesion work is broad and includes some aspects of more anterior regions such as the vmPFC.

We also did not find a strong association between these executive functions and atrophy in a subcortical network evaluated prior to DBS. Although subcortical atrophy has been shown to influence longitudinal atrophic change in prefrontal regions (Zeighami et al., 2015; Yau et al., 2018) we note that this network was defined in *de novo* cases of Parkinson's disease evaluated on average seven months after diagnosis and followed longitudinally one year later. In contrast, our sample were on average eight-years post-diagnosis. Progression of neurodegeneration may have therefore disrupted the specificity of this measure, noting also the small size of our investigation. Nevertheless, it can be hypothesised that those participants with a lower atrophic burden would also show relatively maintained frontal connectivity and hence superior executive functioning longitudinally. This was supported in our cross-lagged model, in which stronger baseline STN-OFC connectivity was protective against pre- to postoperative change in initiation, inhibition and strategy use. Further work with larger sample sizes including participants at an earlier disease stage would be more likely to clarify the relationship between subcortical atrophy and executive dysfunction.

We found that the structural connectivity of our postoperative fronto-subthalamic network (centred upon the VAT) associated far more strongly with variability in postoperative initiation and inhibition than measures of focal subthalamic stimulation derived from a subregion analysis. There are two potential explanations for these findings. First, the structural network measures may allow a more fine-grained measurement of the association between brain and behaviour than the STN subregion data. This is because the STN has an overlapping topography with boundaries that are defined heuristically rather than according to tight criteria (Alkemade and Forstmann, 2014). In order words, the 'motor' subregion will undoubtedly contain some connections to 'associative' cortical regions and vice versa. Secondly, the subthalamic VAT may extend outside of the nucleus to incorporate adjacent fibre tracts projecting to the prefrontal cortex, such as the superolateral branch of the medial forebrain bundle (Coenen et al., 2018), which could conceivably exert a direct influence upon executive functioning. Future work could dissect the relative influence of these factors by constraining a connectivity analysis only to those regions that fall inside of the defined STN boundary, or seeding from other regions of the midbrain such as the ventral tegmental area.

Relatedly, the significance of the association between the connectivity of the stimulation field with the prefrontal cortex and postoperative behaviour may be questioned because, across the cohort, stimulation predominated in the motor subregion of the STN (Fig. 2), which is not typically taken to be strongly connected to these regions. However, the dispersion of charge along the medial and inferior elements of the STN meant that some limbic regions of the STN were directly stimulated (Supplementary Table 2) with a mean occupancy by the VAT of 33.5 % in the right hemisphere and 25.1 % in the left hemisphere. Additionally, the aforementioned overlapping topography of the STN means that

these prefrontal regions will also likely have some representation in associative subregions. Finally, the dispersion of electrical charge outside of the nucleus means that adjacent fibre tracts directly connecting midbrain regions to the prefrontal cortex may be directly recruited.

Limitations of this work include the exclusive focus on verbal measures of initiation and inhibition, which may therefore omit other important behavioural manifestations of these executive functions. However, we have recently reported on behavioural measures of impulsivity derived from a '*virtual casino*' (Mosley et al., 2020), finding here also a key role for STN-OFC tracts in mediating impulsivity after STN-DBS for Parkinson's disease, with clinically-significant pathological changes in mood and behaviour linked to stimulation of these connections in the right hemisphere. Therefore, there appears to be substantial commonality between these constructs. A limitation inherent to almost all work assessing the structural connectivity of the postoperative stimulation field is that this is assayed using diffusion imaging collected preoperatively. Most DBS devices are not approved for the longer sequences required to collect diffusion data at high angular resolution. Therefore, a major assumption is that the structural connectivity of the brain does not substantially change in the pre-postoperative interval. This is a reasonable assumption in cases where the two timepoints surveyed are relatively close together. However, in the future, the development of fully MR compatible devices would remove this necessity and could potentially detect subtle neuroplastic changes emerging after DBS.

5. Conclusions

Overall, these findings support a model in which the integrity of cortico-STN afferent fibres from the anterior prefrontal cortex maintain initiation and inhibition in the context of neurodegeneration, in which the right hemisphere is implicated in strategy use and disinhibition, whilst the left is implicated in selection under conditions of maintained inhibition. The significant postoperative influence of cortical connectivity with the site of subthalamic stimulation, in contrast to local stimulation effects within the nucleus, suggests that it is also important to consider the distal effects of DBS when evaluating individual non-motor symptom outcome in Parkinson's disease. We anticipate that this work will encourage the integration of these network measures into the delivery of DBS. First, quantification of preoperative cortico-STN structural connectivity may hold promise as a marker of neuropsychiatric '*reserve*' mitigating the pro-impulsive effect of STN-DBS. Second, specific tracts connecting the inferomedial STN with the anterior prefrontal cortex (particularly in the right hemisphere) that, when stimulated, are implicated in the genesis of disinhibition, could be incorporated into DBS surgical planning software to guide electrode implantation and stimulation titration to minimise neuropsychiatric sequelae.

Funding agencies

PEM was supported by an early career fellowship from the Queensland government's 'Advance Queensland' initiative, a Royal Brisbane & Woman's Hospital Foundation Research Grant and a young investigator grant from the Royal Australian and New Zealand College of Psychiatrists. He received an unrestricted educational grant from Medtronic. MB was supported by the National Health and Medical Research Council (118153, 10371296, 1095227) and the Australian Research Council (CE140100007). GR was supported by the National Health and Medical Research Council Boosting Dementia Research Leadership Fellowship (APP1135769).

Financial disclosures / conflicts of interest

All authors report no conflict of interest.

CRediT authorship contribution statement

Philip E. Mosley: Conceptualization, Methodology, Formal analysis, Writing - original draft, Visualization. **Katherine Robinson:** Project administration. **Terry Coyne:** Resources. **Peter Silburn:** Resources. **Megan S. Barker:** Supervision. **Michael Breakspear:** Supervision, Writing - review & editing. **Gail A. Robinson:** Conceptualization, Methodology, Writing - review & editing, Supervision. **Alistair Perry:** Conceptualization, Methodology, Writing - review & editing, Supervision.

Acknowledgments

The authors gratefully acknowledge the commitment of participants and caregivers who contributed their time to this study. The authors acknowledge the ongoing support of St Andrew's War Memorial Hospital and the Herston Imaging Research Facility. The authors thank Till Dembek for assistance with modelling the field of stimulation in directional leads and Amelia Ceslis for providing neuropsychology supervision to KR.

Supplementary materials

Supplementary material associated with this article can be found, in the online version, at doi:10.1016/j.neuroimage.2020.117352.

References

Accolla, EA, Dukart, J, Helms, G, Weiskopf, N, Kherif, F, Lutti, A, et al., 2014. Brain tissue properties differentiate between motor and limbic basal ganglia circuits. Hum. Brain Mapp. 35 (10), 5083–5092.

Accolla, EA, Herrojo Ruiz, M, Horn, A, Schneider, GH, Schmitz-Hubsch, T, Draganski, B, et al., 2016. Brain networks modulated by subthalamic nucleus deep brain stimulation. Brain J. Neurol. 139 (Pt 9), 2503–2515.

Akram, H, Sotiropoulos, SN, Jbabdi, S, Georgiev, D, Mahlknecht, P, Hyam, J, et al., 2017. Subthalamic deep brain stimulation sweet spots and hyperdirect cortical connectivity in Parkinson's disease. Neuroimage 158, 332–345.

Alexander, MP, Stuss, DT, Shallice, T, Picton, TW, Gillingham, S, 2005. Impaired concentration due to frontal lobe damage from two distinct lesion sites. Neurology 65 (4), 572–579.

Alkemade, A, Forstmann, BU., 2014. Do we need to revise the tripartite subdivision hypothesis of the human subthalamic nucleus (STN)? Neuroimage 95, 326–329.

Allen, M, Poggiali, D, Whitaker, K, Marshall, T, Kievit, R, 2019. Raincloud plots: a multi-platform tool for robust data visualization [version 1; peer review: 2 approved]. Wellcome Open Res. 4 (63).

Andersson, JLR, Sotiropoulos, SN., 2016. An integrated approach to correction for off-resonance effects and subject movement in diffusion MR imaging. Neuroimage 125, 1063–1078.

Antonelli, F, Ko, JH, Miyasaki, J, Lang, AE, Houle, S, Valzania, F, et al., 2014. Dopamine-agonists and impulsivity in Parkinson's disease: impulsive choices vs. impulsive actions. Hum. Brain Mapp. 35 (6), 2499–2506.

Appleby, BS, Duggan, PS, Regenberg, A, Rabins, PV, 2007. Psychiatric and neuropsychiatric adverse events associated with deep brain stimulation: A meta-analysis of ten years' experience. Mov. Disord. 22 (12), 1722–1728.

Aron, AR, 2011. From reactive to proactive and selective control: developing a richer model for stopping inappropriate responses. Biol. Psychiatry 69 (12), e55–e68.

Aron, AR, Behrens, TE, Smith, S, Frank, MJ, Poldrack, RA, 2007. Triangulating a cognitive control network using diffusion-weighted magnetic resonance imaging (MRI) and functional MRI. J. Neurosci. 27 (14), 3743–3752.

Aron, AR, Monsell, S, Sahakian, BJ, Robbins, TW, 2004a. A componential analysis of task-switching deficits associated with lesions of left and right frontal cortex. Brain 127 (7), 1561–1573.

Aron, AR, Robbins, TW, Poldrack, RA, 2004b. Inhibition and the right inferior frontal cortex. Trends Cognit. Sci. 8 (4), 170–177.

Ash, S, McMillan, C, Gross, RG, Cook, P, Gunawardena, D, Morgan, B, et al., 2012. Impairments of speech fluency in Lewy body spectrum disorder. Brain Lang. 120 (3), 290–302.

Avants, BB, Epstein, CL, Grossman, M, Gee, JC, 2008. Symmetric diffeomorphic image registration with cross-correlation: evaluating automated labeling of elderly and neurodegenerative brain. Med. Image Anal. 12 (1), 26–41.

Barker, MS, Nelson, NL, O'Sullivan, JD, Adam, R, Robinson, GA, 2018. Energization and spoken language production: Evidence from progressive supranuclear palsy. Neuropsychologia 119, 349–362.

Benjamini, Y, Hochberg, Y., 1995. Controlling the false discovery rate: a practical and powerful approach to multiple testing. J. R. Stat. Soc. Ser. B (Methodol.) 57 (1), 289–300.

Blank, SC, Scott, SK, Murphy, K, Warburton, E, Wise, RJS, 2002. Speech production: Wernicke, Broca and beyond. Brain J. Neurol. 125 (8), 1829–1838.

Braun, AR, Guillemin, A, Hosey, L, Varga, M, 2001. The neural organization of discourse: An H215O-PET study of narrative production in English and American sign language. Brain J. Neurol. 124 (10), 2028–2044.
Brown, P, Oliviero, A, Mazzone, P, Insola, A, Tonali, P, Di Lazzaro, V, 2001. Dopamine dependency of oscillations between subthalamic nucleus and pallidum in Parkinson's disease. J. Neurosci. 21 (3), 1033–1038.
Burgess PW, Shallice T, Thames Valley Test Company. The Hayling and Brixton tests. Bury St Edmunds: Thames Valley Test Company; 1997.
Camicioli, R, Gee, M, Bouchard, TP, Fisher, NJ, Hanstock, CC, Emery, DJ, et al., 2009. Voxel-based morphometry reveals extra-nigral atrophy patterns associated with dopamine refractory cognitive and motor impairment in parkinsonism. Parkinsonism Relat. Disord. 15 (3), 187–195.
Cavanagh, JF, Wiecki, TV, Cohen, MX, Figueroa, CM, Samanta, J, Sherman, SJ, et al., 2011. Subthalamic nucleus stimulation reverses mediofrontal influence over decision threshold. Nat. Neurosci. 14 (11), 1462–1467.
Chen, Y, Ge, S, Li, Y, Li, N, Wang, J, Wang, X, et al., 2018. Role of the cortico-subthalamic hyperdirect pathway in deep brain stimulation for the treatment of Parkinson disease: a diffusion tensor imaging study. World Neurosurg. 114, e1079–e1e85.
Cipolotti, L, Healy, C, Spano, B, Lecce, F, Biondo, F, Robinson, G, et al., 2016. Strategy and suppression impairments after right lateral prefrontal and orbito-frontal lesions. Brain J. Neurol. 139 (Pt 2), e10.
Coenen, VA, Honey, CR, Hurwitz, T, Rahman, AA, McMaster, J, Burgel, U, et al., 2009. Medial forebrain bundle stimulation as a pathophysiological mechanism for hypomania in subthalamic nucleus deep brain stimulation for Parkinson's disease. Neurosurgery 64 (6), 1106–1114 discussion 14-5.
Coenen, VA, Panksepp, J, Hurwitz, TA, Urbach, H, Madler, B, 2012. Human medial forebrain bundle (MFB) and anterior thalamic radiation (ATR): imaging of two major subcortical pathways and the dynamic balance of opposite affects in understanding depression. J. Neuropsychiatry Clin. Neurosci. 24 (2), 223–236.
Coenen, VA, Schumacher, LV, Kaller, C, Schlaepfer, TE, Reinacher, PC, Egger, K, et al., 2018. The anatomy of the human medial forebrain bundle: Ventral tegmental area connections to reward-associated subcortical and frontal lobe regions. Neuroimage Clin. 18, 770–783.
Combs, HL, Folley, BS, Berry, DT, Segerstrom, SC, Han, DY, Anderson-Mooney, AJ, et al., 2015. Cognition and depression following deep brain stimulation of the subthalamic nucleus and globus pallidus pars internus in Parkinson's disease: a meta-analysis. Neuropsychol. Rev. 25 (4), 439–454.
Daniele, A, Albanese, A, Contarino, MF, Zinzi, P, Barbier, A, Gasparini, F, et al., 2003. Cognitive and behavioural effects of chronic stimulation of the subthalamic nucleus in patients with Parkinson's disease. J. Neurol. Neurosurg. Psychiatry 74 (2), 175–182.
Daniels, C, Krack, P, Volkmann, J, Pinsker, MO, Krause, M, Tronnier, V, et al., 2010. Risk factors for executive dysfunction after subthalamic nucleus stimulation in Parkinson's disease. Mov. Disord. 25 (11), 1583–1589.
Davatzikos, C., 2004. Why voxel-based morphometric analysis should be used with great caution when characterizing group differences. Neuroimage 23 (1), 17–20.
Doll, BB, Frank, MJ., 2009. Chapter 19 - The basal ganglia in reward and decision making: computational models and empirical studies. In: Dreher, J-C, Tremblay, L (Eds.), Handbook of Reward and Decision Making. Academic Press, New York, pp. 399–425.
Edlow, BL, Mareyam, A, Horn, A, Polimeni, JR, Witzel, T, Tisdall, MD, et al., 2019. 7 Tesla MRI of the ex vivo human brain at 100 micron resolution. Sci. Data 6 (1), 244.
Emre, M, Aarsland, D, Brown, R, Burn, DJ, Duyckaerts, C, Mizuno, Y, et al., 2007. Clinical diagnostic criteria for dementia associated with Parkinson's disease. Mov. Disord. 22 (12), 1689–1707.
Eusebio, A, Pogosyan, A, Wang, S, Averbeck, B, Gaynor, LD, Cantiniaux, S, et al., 2009. Resonance in subthalamo-cortical circuits in Parkinson's disease. Brain J. Neurol. 132 (8), 2139–2150.
Eusebio, A, Thevathasan, W, Doyle Gaynor, L, Pogosyan, A, Bye, E, Foltynie, T, et al., 2011. Deep brain stimulation can suppress pathological synchronisation in parkinsonian patients. J. Neurol. Neurosurg. Psychiatry 82 (5), 569–573.
Evans, AH, Katzenschlager, R, Paviour, D, O'Sullivan, JD, Appel, S, Lawrence, AD, et al., 2004. Punding in Parkinson's disease: its relation to the dopamine dysregulation syndrome. Mov. Disord. 19 (4), 397–405.
Ewert, S, Plettig, P, Li, N, Chakravarty, MM, Collins, DL, Herrington, TM, et al., 2018. Toward defining deep brain stimulation targets in MNI space: A subcortical atlas based on multimodal MRI, histology and structural connectivity. Neuroimage 170, 271–282.
Frank, MJ, Samanta, J, Moustafa, AA, Sherman, SJ, 2007. Hold your horses: impulsivity, deep brain stimulation, and medication in Parkinsonism. Science 318 (5854), 1309–1312.
Fuster, JM., 2015. Chapter 8 - Overview of prefrontal functions: E Pluribus Unum – Coordinating new sequences of purposeful action. In: Fuster, JM (Ed.), The Prefrontal Cortex. Academic Press, San Diego, pp. 375–425.
Gauggel, S, Rieger, M, Feghoff, TA, 2004. Inhibition of ongoing responses in patients with Parkinson's disease. J. Neurol. Neurosurg. Psychiatry 75 (4), 539–544.
Glasser, MF, Coalson, TS, Robinson, EC, Hacker, CD, Harwell, J, Yacoub, E, et al., 2016. A multi-modal parcellation of human cerebral cortex. Nature 536 (7615), 171–178.
Haber, SN, Knutson, B., 2010. The reward circuit: linking primate anatomy and human imaging. Neuropsychopharmacology 35 (1), 4.
Haynes, WI, Haber, SN., 2013. The organization of prefrontal-subthalamic inputs in primates provides an anatomical substrate for both functional specificity and integration: implications for Basal Ganglia models and deep brain stimulation. J. Neurosci. 33 (11), 4804–4814.
Hellerbach, A, Dembek, TA, Hoevels, M, Holz, JA, Gierich, A, Luyken, K, et al., 2018. DiODe: directional orientation detection of segmented deep brain stimulation leads: a sequential algorithm based on CT imaging. Stereotact. Funct. Neurosurg. 96 (5), 335–341.
Hershey, T, Campbell, MC, Videen, TO, Lugar, HM, Weaver, PM, Hartlein, J, et al., 2010. Mapping Go-No-Go performance within the subthalamic nucleus region. Brain J. Neurol. 133 (Pt 12), 3625–3634.
Hershey, T, Revilla, FJ, Wernle, A, Gibson, PS, Dowling, JL, Perlmutter, JS, 2004. Stimulation of STN impairs aspects of cognitive control in PD. Neurology 62 (7), 1110–1114.
Hoehn, MM, Yahr, MD, 1967. Parkinsonism: onset, progression and mortality. Neurology 17 (5), 427–442.
Horn, A, Kuhn, AA., 2015. Lead-DBS: a toolbox for deep brain stimulation electrode localizations and visualizations. Neuroimage 107, 127–135.
Horn, A, Li, N, Dembek, TA, Kappel, A, Boulay, C, Ewert, S, et al., 2019. Lead-DBS v2: Towards a comprehensive pipeline for deep brain stimulation imaging. Neuroimage 184, 293–316.
Horn, A, Reich, M, Vorwerk, J, Li, N, Wenzel, G, Fang, Q, et al., 2017. Connectivity Predicts deep brain stimulation outcome in Parkinson disease. Ann. Neurol. 82 (1), 67–78.
Hughes, AJ, Daniel, SE, Kilford, L, Lees, AJ, 1992. Accuracy of clinical diagnosis of idiopathic Parkinson's disease: a clinico-pathological study of 100 cases. J. Neurol. Neurosurg. Psychiatry 55 (3), 181–184.
Jahanshahi, M, Obeso, I, Baunez, C, Alegre, M, Krack, P, 2015. Parkinson's disease, the subthalamic nucleus, inhibition, and impulsivity. Mov. Disord. 30 (2), 128–140.
Jbabdi, S, Sotiropoulos, SN, Haber, SN, Van Essen, DC, Behrens, TE, 2015. Measuring macroscopic brain connections in vivo. Nat. Neurosci. 18 (11), 1546–1555.
Jeurissen, B, Tournier, JD, Dhollander, T, Connelly, A, Sijbers, J, 2014. Multi-tissue constrained spherical deconvolution for improved analysis of multi-shell diffusion MRI data. Neuroimage 103, 411–426.
Kievit, RA, Brandmaier, AM, Ziegler, G, van Harmelen, AL, de Mooij, SMM, Moutoussis, M, et al., 2018. Developmental cognitive neuroscience using latent change score models: A tutorial and applications. Dev. Cognit. Neurosci. 33, 99–117.
Kobayakawa, M, Koyama, S, Mimura, M, Kawamura, M, 2008. Decision making in Parkinson's disease: analysis of behavioral and physiological patterns in the Iowa gambling task. Mov. Disord. 23 (4), 547–552.
Krack, P, Batir, A, Van Blercom, N, Chabardes, S, Fraix, V, Ardouin, C, et al., 2003. Five-year follow-up of bilateral stimulation of the subthalamic nucleus in advanced Parkinson's disease. N. Engl. J. Med. 349 (20), 1925–1934.
Lambert, C, Zrinzo, L, Nagy, Z, Lutti, A, Hariz, M, Foltynie, T, et al., 2012. Confirmation of functional zones within the human subthalamic nucleus: patterns of connectivity and sub-parcellation using diffusion weighted imaging. Neuroimage 60 (1), 83–94.
Lee, JE, Park, HJ, Song, SK, Sohn, YH, Lee, JD, Lee, PH, 2010. Neuroanatomic basis of amnestic MCI differs in patients with and without Parkinson disease. Neurology 75 (22), 2009–2016.
Lees, AJ, Smith, E., 1983. Cognitive deficits in the early stages of Parkinson's disease. Brain J. Neurol. 106 (Pt 2), 257–270.
Lin, HY, Perry, A, Cocchi, L, Roberts, JA, Tseng, WI, Breakspear, M, et al., 2019. Development of frontoparietal connectivity predicts longitudinal symptom changes in young people with autism spectrum disorder. Transl. Psychiatry 9 (1), 86.
Mallet, L, Schupbach, M, N'Diaye, K, Remy, P, Bardinet, E, Czernecki, V, et al., 2007. Stimulation of subterritories of the subthalamic nucleus reveals its role in the integration of the emotional and motor aspects of behavior. PNAS 104 (25), 10661–10666.
McAuley, JH., 2003. The physiological basis of clinical deficits in Parkinson's disease. Prog. Neurobiol. 69 (1), 27–48.
McIntosh, AR, Lobaugh, NJ., 2004. Partial least squares analysis of neuroimaging data: applications and advances. Neuroimage 23 (Suppl 1), S250–S263.
Mosley, P, Paliwal, S, Robinson, K, Coyne, T, Silburn, P, Tittgemeyer, M, et al., 2020. The structural connectivity of subthalamic deep brain stimulation correlates with impulsivity in Parkinson's. Brain 143 (7), 2235–2254.
Mosley, PE, Marsh, R., 2015. The psychiatric and neuropsychiatric symptoms after subthalamic stimulation for Parkinson's disease. J. Neuropsychiatry Clin. Neurosci. 27 (1), 19–26.
Mosley, PE, Marsh, R, Perry, A, Coyne, T, Silburn, P, 2018a. Persistence of mania after cessation of stimulation following subthalamic deep brain stimulation. J. Neuropsychiatry Clin. Neurosci. 30 (3), 246–249.
Mosley, PE, Paliwal, S, Robinson, K, Coyne, T, Silburn, P, Tittgemeyer, M, et al., 2019. The structural connectivity of discrete networks underlies impulsivity and gambling in Parkinson's disease. Brain 142 (12), 3917–3935.
Mosley, PE, Smith, D, Coyne, T, Silburn, P, Breakspear, M, Perry, A, 2018b. The site of stimulation moderates neuropsychiatric symptoms after subthalamic deep brain stimulation for Parkinson's disease. NeuroImage Clin. 18, 996–1006.
Muetzel, RL, Blanken, LME, van der Ende, J, El Marroun, H, Shaw, P, Sudre, G, et al., 2018. Tracking brain development and dimensional psychiatric symptoms in children: a longitudinal population-based neuroimaging study. Am. J. Psychiatry 175 (1), 54–62.
Nambu, A, Tokuno, H, Hamada, I, Kita, H, Imanishi, M, Akazawa, T, et al., 2000. Excitatory cortical inputs to pallidal neurons via the subthalamic nucleus in the monkey. J. Neurophysiol. 84 (1), 289–300.
Nishio, Y, Hirayama, K, Takeda, A, Hosokai, Y, Ishioka, T, Suzuki, K, et al., 2010. Corticolimbic gray matter loss in Parkinson's disease without dementia. Eur. J. Neurol. Off. J. Eur. Fed. Neurol. Soc. 17 (8), 1090–1097.
Nombela, C, Rittman, T, Robbins, TW, Rowe, JB, 2014. Multiple modes of impulsivity in Parkinson's disease. PLoS One 9 (1), e85747.
O'Callaghan, C, Naismith, SL, Hodges, JR, Lewis, SJ, Hornberger, M, 2013a. Fronto-striatal atrophy correlates of inhibitory dysfunction in Parkinson's disease versus behavioural variant frontotemporal dementia. Cortex 49 (7), 1833–1843.
O'Callaghan, C, Naismith, SL, Shine, JM, Bertoux, M, Lewis, SJ, Hornberger, M, 2013b. A novel bedside task to tap inhibitory dysfunction and fronto-striatal atrophy in Parkinson's disease. Parkinsonism Relat. Disord. 19 (9), 827–830.
Obeso, I, Wilkinson, L, Casabona, E, Bringas, ML, Alvarez, M, Alvarez, L, et al., 2011. Deficits in inhibitory control and conflict resolution on cognitive and motor tasks in Parkinson's disease. Exp. Brain Res. 212 (3), 371–384.

Obeso, I, Wilkinson, L, Rodriguez-Oroz, MC, Obeso, JA, Jahanshahi, M, 2013. Bilateral stimulation of the subthalamic nucleus has differential effects on reactive and proactive inhibition and conflict-induced slowing in Parkinson's disease. Exp. Brain Res. 226 (3), 451–462.

Parsons, TD, Rogers, SA, Braaten, AJ, Woods, SP, Troster, AI, 2006. Cognitive sequelae of subthalamic nucleus deep brain stimulation in Parkinson's disease: a meta-analysis. Lancet Neurol. 5 (7), 578–588.

Picton, TW, Stuss, DT, Alexander, MP, Shallice, T, Binns, MA, Gillingham, S, 2007. Effects of focal frontal lesions on response inhibition. Cereb. Cortex 17 (4), 826–838.

Rae, CL, Correia, MM, Altena, E, Hughes, LE, Barker, RA, Rowe, JB, 2012. White matter pathology in Parkinson's disease: the effect of imaging protocol differences and relevance to executive function. Neuroimage 62 (3), 1675–1684.

Rae, CL, Hughes, LE, Anderson, MC, Rowe, JB, 2015. The prefrontal cortex achieves inhibitory control by facilitating subcortical motor pathway connectivity. J. Neurosci. 35 (2), 786–794.

Raffelt, D, Tournier, JD, Rose, S, Ridgway, GR, Henderson, R, Crozier, S, et al., 2012. Apparent Fibre Density: a novel measure for the analysis of diffusion-weighted magnetic resonance images. Neuroimage 59 (4), 3976–3994.

Robinson, G, Shallice, T, Bozzali, M, Cipolotti, L, 2010. Conceptual proposition selection and the LIFG: neuropsychological evidence from a focal frontal group. Neuropsychologia 48 (6), 1652–1663.

Robinson, G, Shallice, T, Bozzali, M, Cipolotti, L, 2012. The differing roles of the frontal cortex in fluency tests. Brain J. Neurol. 135 (Pt 7), 2202–2214.

Robinson, GA, Cipolotti, L, Walker, DG, Biggs, V, Bozzali, M, Shallice, T, 2015a. Verbal suppression and strategy use: a role for the right lateral prefrontal cortex? Brain J. Neurol. 138 (Pt 4), 1084–1096.

Robinson, GA, Spooner, D, Harrison, WJ, 2015b. Frontal dynamic aphasia in progressive supranuclear palsy: Distinguishing between generation and fluent sequencing of novel thoughts. Neuropsychologia 77, 62–75.

Romito, LM, Raja, M, Daniele, A, Contarino, MF, Bentivoglio, AR, Barbier, A, et al., 2002. Transient mania with hypersexuality after surgery for high frequency stimulation of the subthalamic nucleus in Parkinson's disease. Mov. Disord. 17 (6), 1371–1374.

Schuepbach, WM, Rau, J, Knudsen, K, Volkmann, J, Krack, P, Timmermann, L, et al., 2013. Neurostimulation for Parkinson's disease with early motor complications. N. Engl. J. Med. 368 (7), 610–622.

Shallice, T, Stuss, DT, Alexander, MP, Picton, TW, Derkzen, D, 2008. The multiple dimensions of sustained attention. Cortex 44 (7), 794–805.

Shallice, T, Stuss, DT, Picton, TW, Alexander, MP, Gillingham, S, 2007. Multiple effects of prefrontal lesions on task-switching. Front. Hum. Neurosci. 1, 2.

Shaw, P, Weingart, D, Bonner, T, Watson, B, Park, MT, Sharp, W, et al., 2016. Defining the neuroanatomic basis of motor coordination in children and its relationship with symptoms of attention-deficit/hyperactivity disorder. Psychol. Med. 46 (11), 2363–2373.

Shimamoto, SA, Ryapolova-Webb, ES, Ostrem, JL, Galifianakis, NB, Miller, KJ, Starr, PA, 2013. Subthalamic nucleus neurons are synchronized to primary motor cortex local field potentials in Parkinson's disease. J. Neurosci. 33 (17), 7220–7233.

Smith, SM, Jenkinson, M, Woolrich, MW, Beckmann, CF, Behrens, TE, Johansen-Berg, H, et al., 2004. Advances in functional and structural MR image analysis and implementation as FSL. Neuroimage 23 (Suppl 1), S208–S219.

Song, SK, Lee, JE, Park, HJ, Sohn, YH, Lee, JD, Lee, PH, 2011. The pattern of cortical atrophy in patients with Parkinson's disease according to cognitive status. Mov. Disord. 26 (2), 289–296.

Spiegel, J, Hellwig, D, Samnick, S, Jost, W, Mollers, MO, Fassbender, K, et al., 2007. Striatal FP-CIT uptake differs in the subtypes of early Parkinson's disease. J. Neural Transm. 114 (3), 331–335.

Starkstein, SE, Brockman, S., 2011. Apathy and Parkinson's disease. Curr. Treat. Opt. Neurol. 13 (3), 267–273.

Starkstein, SE, Mayberg, HS, Preziosi, TJ, Andrezejewski, P, Leiguarda, R, Robinson, RG, 1992. Reliability, validity, and clinical correlates of apathy in Parkinson's disease. J. Neuropsychiatry Clin. Neurosci. 4 (2), 134.

Stuss, DT, Alexander, MP, Shallice, T, Picton, TW, Binns, MA, Macdonald, R, et al., 2005. Multiple frontal systems controlling response speed. Neuropsychologia 43 (3), 396–417.

Thobois, S, Ardouin, C, Lhommee, E, Klinger, H, Lagrange, C, Xie, J, et al., 2010. Non-motor dopamine withdrawal syndrome after surgery for Parkinson's disease: predictors and underlying mesolimbic denervation. Brain J. Neurol. 133 (Pt 4), 1111–1127.

Tournier, JD, Calamante, F, Connelly, A, 2007. Robust determination of the fibre orientation distribution in diffusion MRI: non-negativity constrained super-resolved spherical deconvolution. Neuroimage 35 (4), 1459–1472.

Tournier, JD, Calamante, F, Connelly, A, 2010. Improved probabilistic streamlines tractography by 2nd order integration over fibre orientation distributions. Proc. Int. Soc. Magn. Reson. Med. Stockh..

Tournier, JD, Calamante, F, Gadian, DG, Connelly, A, 2004. Direct estimation of the fiber orientation density function from diffusion-weighted MRI data using spherical deconvolution. Neuroimage 23 (3), 1176–1185.

van der Vegt, JP, Hulme, OJ, Zittel, S, Madsen, KH, Weiss, MM, Buhmann, C, et al., 2013. Attenuated neural response to gamble outcomes in drug-naive patients with Parkinson's disease. Brain 136 (Pt 4), 1192–1203.

van Langen J. Open-visualizations in R and Python (Version v.1.0.4). 2020.

Vanegas-Arroyave, N, Lauro, PM, Huang, L, Hallett, M, Horovitz, SG, Zaghloul, KA, et al., 2016. Tractography patterns of subthalamic nucleus deep brain stimulation. Brain J. Neurol. 139 (Pt 4), 1200–1210.

Veraart, J, Novikov, DS, Christiaens, D, Ades-Aron, B, Sijbers, J, Fieremans, E, 2016. Denoising of diffusion MRI using random matrix theory. Neuroimage 142, 394–406.

Vila, M, Perier, C, Feger, J, Yelnik, J, Faucheux, B, Ruberg, M, et al., 2000. Evolution of changes in neuronal activity in the subthalamic nucleus of rats with unilateral lesion of the substantia nigra assessed by metabolic and electrophysiological measurements. Eur. J. Neurosci. 12 (1), 337–344.

Volkmann, J, Daniels, C, Witt, K, 2010. Neuropsychiatric effects of subthalamic neurostimulation in Parkinson disease. Nat. Rev. Neurol. 6 (9), 487–498.

Volle, E, de Lacy Costello, A, Coates, LM, McGuire, C, Towgood, K, Gilbert, S, et al., 2012. Dissociation between verbal response initiation and suppression after prefrontal lesions. Cereb. Cortex 22 (10), 2428–2440.

Voon, V, Kubu, C, Krack, P, Houeto, JL, Troster, AI, 2006. Deep brain stimulation: neuropsychological and neuropsychiatric issues. Mov. Disord. 21 (Suppl 14), S305–S327.

Warrington, EK., 2010. The Queen Square screening test for cognitive deficits: Institute of Neurology.

Weintraub, D, Burn, DJ, 2011. Parkinson's disease: the quintessential neuropsychiatric disorder. Mov. Disord. 26 (6), 1022–1031.

Welter, ML, Schupbach, M, Czernecki, V, Karachi, C, Fernandez-Vidal, S, Golmard, JL, et al., 2014. Optimal target localization for subthalamic stimulation in patients with Parkinson disease. Neurology 82 (15), 1352–1361.

Williams, A, Gill, S, Varma, T, Jenkinson, C, Quinn, N, Mitchell, R, et al., 2010. Deep brain stimulation plus best medical therapy versus best medical therapy alone for advanced Parkinson's disease (PD SURG trial): a randomised, open-label trial. Lancet Neurol. 9 (6), 581–591.

Witt, K, Daniels, C, Reiff, J, Krack, P, Volkmann, J, Pinsker, MO, et al., 2008. Neuropsychological and psychiatric changes after deep brain stimulation for Parkinson's disease: a randomised, multicentre study. Lancet Neurol. 7 (7), 605–614.

Witt, K, Granert, O, Daniels, C, Volkmann, J, Falk, D, van Eimeren, T, et al., 2013. Relation of lead trajectory and electrode position to neuropsychological outcomes of subthalamic neurostimulation in Parkinson's disease: results from a randomized trial. Brain J. Neurol. 136 (Pt 7), 2109–2119.

Xia, M, Wang, J, He, Y, 2013. BrainNet Viewer: a network visualization tool for human brain connectomics. PLoS One 8 (7), e68910.

Yau, Y, Zeighami, Y, Baker, TE, Larcher, K, Vainik, U, Dadar, M, et al., 2018. Network connectivity determines cortical thinning in early Parkinson's disease progression. Nat. Commun. 9 (1), 12.

Zeighami, Y, Ulla, M, Iturria-Medina, Y, Dadar, M, Zhang, Y, Larcher, KM, et al., 2015. Network structure of brain atrophy in de novo Parkinson's disease. Elife 4.

Zhang, Y, Brady, M, Smith, S, 2001. Segmentation of brain MR images through a hidden Markov random field model and the expectation-maximization algorithm. IEEE Trans. Med. Imaging 20 (1), 45–57.